INVESTIGATION OF MIGRATION OF BREAST CANCER CELLS IN RELATION TO FIBROBLASTS ON A MICROFLUIDIC SYSTEM

A THESIS SUBMITTED TO
THE GRADUATE SCHOOL OF NATURAL AND APPLIED SCIENCES
OF
MIDDLE EAST TECHNICAL UNIVERSITY

BY

CAN ILDIZ

IN PARTIAL FULFILLMENT OF THE REQUIREMENTS
FOR
THE DEGREE OF MASTER OF SCIENCE
IN
MOLECULER BIOLOGY AND GENETICS

AUGUST 2024

Approval of the thesis:

INVESTIGATION OF MIGRATION OF BREAST CANCER CELLS IN RELATION TO FIBROBLASTS ON A MICROFLUIDIC SYSTEM

submitted by **CAN ILDIZ** in partial fulfillment of the requirements for the degree of **Master of Science** in **Molecular Biology and Genetics, Middle East Technical University** by,

Prof. Dr. Naci Emre Altun
Dean, **Graduate School of Natural and Applied Sciences** _____

Prof. Dr. Mesut Muyan
Head of the Department, **Biology,** _____

Assoc. Prof. Dr. Ahmet Acar
Supervisor, **Biology, METU** _____

Assist. Prof. Dr. Altuğ Özçelikkale
Co-Supervisor, **Mechanical Engineering, METU** _____

Examining Committee Members:

Prof. Dr. Pelin Mutlu
Biotechnology, Ankara University _____

Assoc. Prof. Dr. Ahmet Acar
Biology, METU _____

Assist. Prof. Dr. Emine Ertekin Yıldızcan
Biology, METU _____

Date:

23.08.2024

I hereby declare that all information in this document has been obtained and presented in accordance with academic rules and ethical conduct. I also declare that, as required by these rules and conduct, I have fully cited and referenced all material and results that are not original to this work.

Name Last name: Can Ildız

Signature :

ABSTRACT

INVESTIGATION OF MIGRATION OF BREAST CANCER CELLS IN RELATION TO FIBROBLASTS ON MICROFLUIDIC SYSTEM

Ildız, Can
Master of Science, Molecular Biology and Genetics
Supervisor : Assoc. Dr. Ahmet Acar
Co-Supervisor: Assist. Prof. Dr. Altuğ Özçelikkale

August 2024, 70 pages

Breast cancer is one of the most common and deadliest types of cancer in the world. Even though it has been studied in the past, the need for a suitable model system mimicking the disease progression and underlying mechanisms of it are still not clear. Current status quo is centred around animal models, which is hard to handle, economically unfeasible and raise ethical concerns for researchers. Therefore, we have developed a microfluidic system that utilizes breast cancer cell lines and fibroblast cells to mimic the tumour microenvironment. Since the cancer related deaths, in most cases, occur as a result of metastasis, we aimed to adapt our proposed microfluidic system to investigate migratory phenotypes of cancer cells in relation to fibroblasts. The migration of breast cancer cells from the microfluidic micro-chamber towards the micro-channel was examined in order to understand the metastatic potential of cancer cells. To do so, the migration was studied in the presence and absence of fibroblasts using our own microfluidic system which was also developed as part of this project. As a result, this system did provide a relatively economical, practical and reasonable model to study the migration of breast cancer cells facilitated by fibroblasts.

Keywords: Microfluidics, Fibroblasts, Cancer, Migration.

ÖZ

MİKROAKIŞKAN SİSTEMDE MEME KANSERİ HÜCRELERİNİN FİBROBLASTLARA GÖRELİ MİGRASYONUNUN İNCELENMESİ

ILDIZ, Can
Yüksek Lisans, Moleküler Biyoloji ve Genetik
Tez Yöneticisi: Doç. Dr. Ahmet Acar
Ortak Tez Yöneticisi: Dr. Öğr. Üyesi Altuğ Özçelikkale

Ağustos 2024

Meme kanseri, dünya üzerindeki en yaygın ve ölümcül kanser türlerinden biridir. Geçmişte çalışılmış olmasına karşın, hastalığın gelişimi ve altyapısındaki mekanizmaları gösterebilen uygun bir model sistem hala daha geliştirilmemiştir.Günümüzdeki statüko, genel olarak kullanılması zor, ekonomik olarak yıpratıcı ve ahlaki açıdan problemli olan hayvan modelleri etrafında konumlanmıştır. Bu nedenle meme kanseri hücre hatları ve fibroblastları kullanarak tümör mikroçevresini taklit eden bir sistem geliştirmeyi planlıyoruz. Genelde, çok büyük oranla, kanser nedenli ölümler metastaz sonucunda meydana gelmektedir. Bu nedenle tasarladığımız mikroakışkan sistem, kanser hücrelerinin fibroblastlara göreli migrasyon davranışını inceleyecek şekilde tasarlandı. Bu inceleme esnasındaki nihai hedefimiz, kanser hücrelrinin migrasyon davranışının fibroblastlara göre değişimini ortaya koymuş olduk. Meme kanseri hücrelerinin, mikro rezervuardan mikro-kanala migrasyonu, bu hücrelerin metastatik potansiyelini anlamak için araştırıldı. Bunu gerçekleştirebilmek adına da, tasarladığımız mikrofluidik sistem fibroblastların varlığı ve yokluğunda incelendi. Sonuç olarak, geliştirdiğimiz sistem fibroblast merkezli meme kanseri migrasyonunu araştırmak için pratik, mantıklı ve görece ekonomik bir model öne sürmüş olmaktadır.

Anahtar Kelimeler: Mikroakışkan, Fibroblast, Kanser, Migrasyon

This thesis is dedicated to every name in history who, without hesitation, has committed an entire life to the pursuit of science and enlightenment.

ACKNOWLEDGMENTS

I would like to acknowledge my thesis supervisor Assoc. Dr. Ahmet Acar for his guidance, mentorship, criticism, help and support in this project and express my deepest appreciation and respect. I would also like to express my sincerest thanks to my co-advisor Dr. Altuğ Özçelikkale for his help and assistance in this research. I am very grateful for his dedication on this project.

I would like to thank my thesis examination committee members Prof. Dr. Pelin Mutlu and Assist. Prof. Dr. Emine Ertekin Yıldızcan for their time and effort devoted to this project.

I would like to present my thanks to my colleagues in Acar Lab; Tuğçe Dilber, Kübra Çelikbaş Yılmaz and Safa Kerem Aydın for their help to my study.

I wish to express my deepest gratitude and appreciation to my friends, advisors and colleagues Hakan Berk Aydın and Gizem Damla Yalçın for both their academic and emotional support throughout the project.

I would like to thank past and present Özçelikkale Lab members; Ali Mehrasa, Milad Fathi and Barış Dedekargınoğlu for their support, with special thanks to Barış Dedekargınoğlu and Milad Fathi for their active participation and help in this research.

Finally I wish to present my profound thanks to my family for supporting me in every area of life, including science.

This work is partially, financially supported by Scientific and Technological Research Council of Turkey's (TUBITAK) BIDEB2210A scholarship.

TABLE OF CONTENTS

LIST OF TABLES

TABLES

LIST OF FIGURES

LIST OF ABBREVIATIONS

ABBREVIATIONS

CAF Cancer-Associated Fibroblast

DMSO Dimethyl Sulfoxide

ECM Extra Cellular Matrix

PDMS Polydimethylsiloxane

PBS Phosphate Buffered Saline

SDS Sodium Dodecyl Sulfate

IPA Isopropyl Alcohol

GFP Green Flourescent Protein

RFP Red Flourescent Protein

3D 3 Dimensional

2D 2 Dimensional

CHAPTER 1

INTRODUCTION

1.1 Microfluidic Systems

The science of microfluidics is defined as the branch of science that investigates flow in artificial miniaturized systems (Atkins & Escudier, 2013). Microfluidic systems are in a scale between 100nm to 100μm. There are various benefits of implementing microfluidic systems over conventional models. Firstly, since the dimensions of microfluidic systems are much smaller than conventional systems, the diffusion time of molecules are much shorter, resulting in a shorter reaction time. In addition, since they require much less amounts of reagents, economical and practical advantages of microfluidics outshine conventional models again (Convery & Gadegaard, 2019).

There are many different areas of research and development that recruit the usage of microfluidic models such as point of care systems, biosensors, lab-on-a-chip development and organ-on-a-chip models. Thus, cancer research in microfluidic systems is a very actively growing field. Cancer cell invasion, intravasation/extravasation and tumour microenvironment are amongst the most studied areas of cancer in terms of microfluidics (Gharib et al., 2022).

Microfluidic devices also hold a great potential for generating fast and non-invasive diagnostic tools. Biomarkers related to cancer such as miRNAs, circulating tumour cells (CTCs), proteins and DNA can be caught and identified via using microfluidic devices. High detection and purification capabilities of microfluidic systems are advantageous in this context since these biomarkers are

usually very low in abundance compared to background noise (Zhang & Nagrath, 2013)

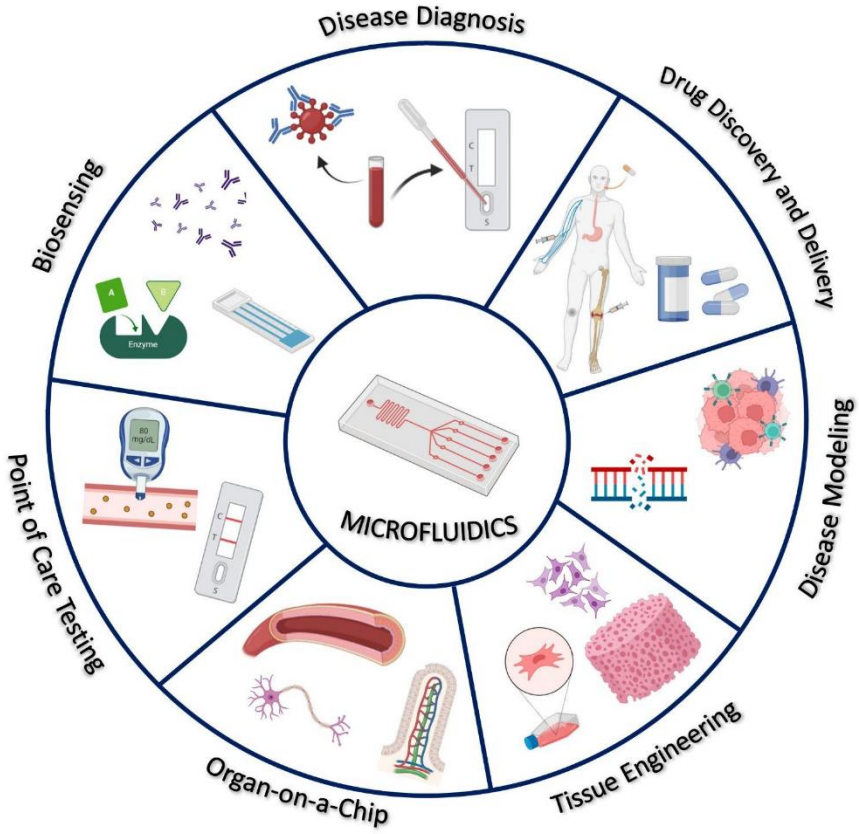

Figure 1.1 Schematic representation of areas that employ microfluidics (taken from (Gharib et al., 2022)).

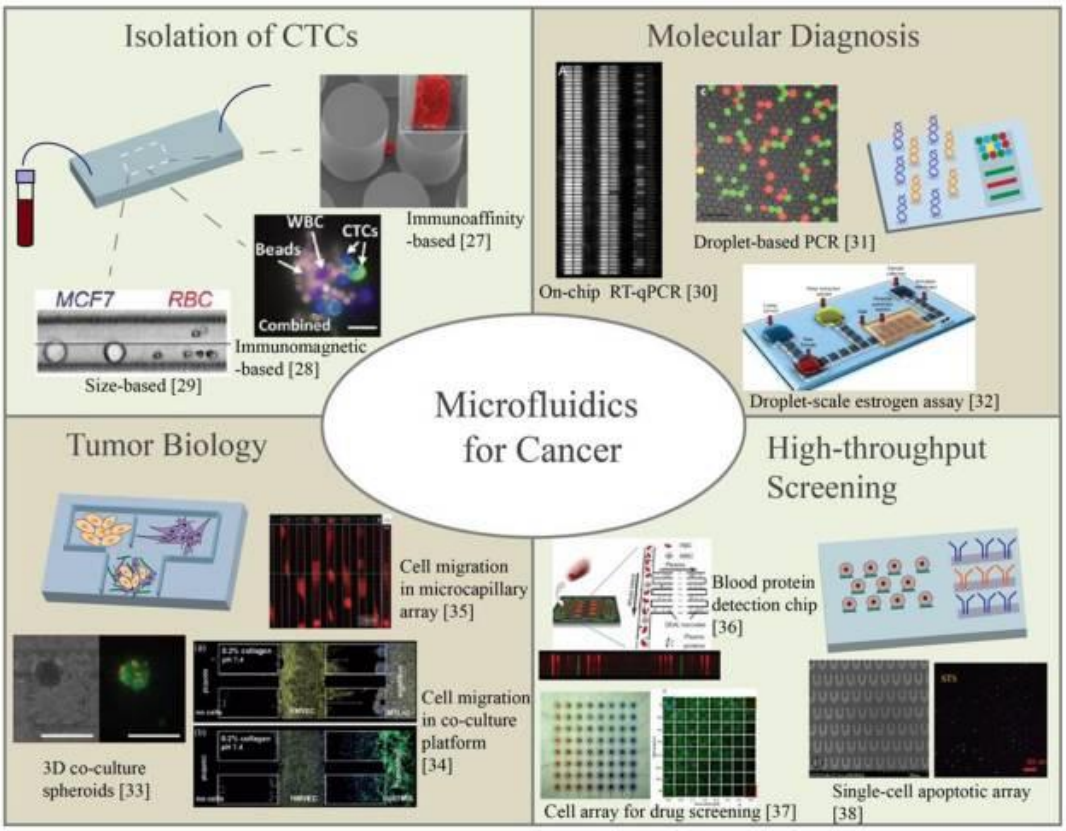

Figure 1.2 Uses of microfluidics in cancer research and diagnosis (taken from Zhang & Nagrath, 2013)).

1.2 Microfluidic Device Manufacturing Techniques

Through time, many different materials such as silicone, glass or quartz have been used to produce microfluidic devices, however polymers such as PDMS or PMMA are favoured currently. In order to more efficiently use time and resources, a master-mould and a cast device manner is used to produce such devices.

There are many different methods to produce these master moulds, each with different pros and cons. There are both mechanical methods such as micro-cutting and ultrasonic machining and energy assisted methods such as laser ablation and electro discharge machining. However, 3D printing is one of the preferred methods

for low volume manufacturing. Since it is affordable, fast and practical to use (Scott & Ali, 2021). 3D printed mold fabrication for microfluidic devices is a relatively new concept that does offer some advantages that conventional methods such as soft lithography don't. For instance, design files for 3D printed microfluidic molds are easily editable, allowing rapid production and testing. Secondly, 3D printing does not require a cleanroom to operate instead of techniques such as photolithography, which can be expensive to install and operate. Thirdly, the consumable materials for 3D printing of microfluidic devices are relatively more economical when compared to materials used for other methods of manufacturing. Finally, 3D printers can produce molds that use all 3-dimensional features (Nielsen et al., 2020). Due to all these reasons, 3D fabrication of microfluidic molds is a promising method that might enable new development in this area. However, it does not come without any setbacks. For example, other methods like soft lithography do present a higher resolution, generally offer higher gas permeability and light transparency (Bhattacharjee et al., 2016).

All the microchips used in this project were produced by using 3D stereolithography method. Thus, it will be shown that mono and multi cell cultures can be done on microfluidic devices that are manufactured by 3D printing for enlengthened periods of time (1-7 days).

Polydimethylsiloxane (PDMS) is a material that is classified as a silicon elastomer. It constitutes of inorganic chains with high surface energy, surrounded by silicates, methyl groups and other inorganics with low surface energy. This structure of PDMS makes it hydrophobic which is an important attribute for microfluidic usage (Ribeiro et. al, 2021). Its features such as being flexible, transparent, non-toxic and being stable are amongst the reasons it is commonly preferred. The unit material cost of PDMS is also lower than its alternatives such as silicon or glass. PDMS also offers high biocompatibility. Since it is perfectly transparent, it allows optical research and experimentation (Lin & Chung, 2021).

Due to it being biocompatible, optically transparent and economically sustainable to produce, PDSM is also widely used in fields such as DNA sequencing, drug delivery, point of care systems and diagnostics (especially with their intersects with microfluidics). Beyond microfluidics, PDMS is also commonly used in hemodynamic models to mimic biological systems such as arteries and veins. (Miranda et. al, 2021).

1.3 Cancer Research Utilizing Microfluidic Devices

Microfluidic technologies are being commonly used in cancer research. They do offer a wide array of different applications. For example, microfluidic devices can be used as diagnostic tools as mentioned before. Circulating tumour cells (CTCs) are cancer cells that are dissociated from primary tumour site and got involved in the blood or lymphatic system. These cells can give a useful diagnostic for cancer; however they are most usually are present in very low quantities in blood, and thus difficult to detect. However, microfluidic tools are a promising idea to perform diagnostic by catching these CTCs.

Moreover, studying cancer cell phenotype on microfluidic chips is one another application. Metastatic patterns of mechanical properties of cancer cells can be studied on microchips. They can also be used for drug screening since they offer a high-throughput manner of experimentation. Angiogenesis, tumour microenvironment and organ-on-a-chip models are also among the most widespread areas of cancer research utilizing microfluidics (Regmi et al, 2022).

Besides these, drug screening studies can be done on microfluidic chips in a fast and economically plausible way. Sampling different tumour tissues on a PDMS microchip and testing different drugs can be done on a microfluidic chip, which is faster and more economical when compared to more conventional methods (Zhai et al., 2024).

It is also possible to culture cancer cells with other types of cells to investigate the interactions between them. For example, devices that allow growing cancer cell spheroids among with cancer-associated fibroblasts (CAFs) have been developed by Jeong et al. (2016).

A soft lithography manufactured microfluidic chip was used to show the migration of breast cancer cells towards different tissue samples (Firatligil-Yildirir et al., 2021).

Moreover, Azadi et al. (2020) used an AIM biotech microchip (produced by soft lithography), similar to the constant width co-culture chip in this project (Figure 2.6.1), to investigate the effects of matrix stiffness on extravasation of MCF7 and MDA-MB-231 cells. To simulate the matrix stiffness, the area between cells and extravasation channel has been filled with differing concentrations of collagen gel.

Parsian et al. (2022) used a microfluidic device to culture breast cancer tissues e*x vivo.* Knock-down mouse models were injected with breast cancer cells MDA-MB-231 and SKBR-3. Afterwards tumour tissues were removed from the mice and cultured in the microfluidic device.

In order to investigate the mechanics of cancer metastasis, Truong et al. (2019) used a photolithography produced microfluidic chip and patient derived cancer associated fibroblasts (CAFs). They've concluded that CAFs enhance the invasive behaviour of breast cancer cells in a 3D microfluidic model.

Vasudevan et al. (2020), again used a photolithographically produced microfluidic device to investigate the effect of matrix stiffness in cancer migration.

To sum up, it can be said that there are many different studies that utilizes microfluidic devices to study the different aspects of cancer migration. However, a common trend seen in almost all these studies is that they employ micro devices produced with more conventional methods, mostly being photolithography.

1.4 Cancer Cell Migration and Metastasis

Cancer cell migration and invasion are steps in the phenomenon called metastasis, which is responsible for the greatest number of deaths in cancer patients. In order for cancer cells to detach from primary tumour mass, they need to become malignant and break the basal membrane. Afterwards, they penetrate the extracellular matrix (ECM) and involved in the circulation, which is named as intravasation. Cellular migration can happen both in a single cell or collective manner.

Single cell migration can be categorized in two different ways. The first one is amoeboid cell migration, which has features such as high cellular motility, deformable cell morphology, weak ECM interactions and no proteolytic degradation of matrix. On the other hand, mesenchymal cell migration depends on the proteolytic degradation of matrix. These kinds of cells display mesenchymal morphology such as elongated cell outline (Wu et al, 2020).

The second principal mode of migration of cancer cells, is the collective migration. In this case, cells move as sheets, clusters or ducts in contrast to moving individually. There are several hallmarks of collective migration. Firstly, cells remain physically and functionally connected throughout the movement. Then, the polarity of actin cytoskeleton remains intact and generate protrusion/traction force. Thirdly, in most cases of collective migration the moving group of cells modify the ECM (Friedl & Gilmour, 2009).

Genomic instability and mutations cause cancer cell to gain a migratory behaviour and eventually metastasize to other sites. The exact mechanism relating genetic alterations to cancer cell migration is not exactly understood. However, more and more evidence point to the idea that some mutations might trigger or accelerate the migration of cancer cells (Novikov et al., 2020).

As previously mentioned, ECM remodelling is an important step in metastasis and migration. Enzymes called matrix metalloproteinases (MMPs) are the major players

in ECM degradation and remodelling. In many cases of cancer, an elevation of MMPs is observed and related with poor prognosis of disease (Fares et al., 2020).

Cancer migration can be studied in both 2 dimensional and 3-dimensional culture systems. In 2-dimensional growth cultures, cells grow as a monolayered sheet, attached to a flat surface. The main advantages of 2D cultures are ease of use and low cost. However, they endure some limitations. For example, they do not mimic the actual tumour environment since they lack the natural structures and forces found in the tumour. To overcome these problems, 3D cultures were developed. In such systems, cells can grow and move in all spatial dimensions, resembling an actual biological sample. There are various systems for 3D cell cultures such as hanging drop spheroids, gel-based assays and some microfluidic systems (Kapałczyńska et al., 2016).

1.5 Fibroblasts And Cancer

Fibroblasts are mesenchymal cells that are adapted for different niches and purposes. They do get involved in homeostasis and extra cellular matrix production. They are one of the most major players in supporting and forming the connective tissue, thus getting involved in many different functions such as breathing and resistance to trauma. They also act as progenitors for some cells such as osteoblasts and adipocytes. So basically, they both serve as constructors of extracellular matrix and signalling intermediates for some types of cells. They also take part in immune function, performing tasks such as macrophage polarization, cytokine synthesis and antimicrobial peptide synthesis. The fibroblasts are also employed to remodel surrounding matrix and tissue (Plikus et al, 2021).

Cancer-associated fibroblasts (CAFs), on the other hand, mostly take part in the tumour microenvironment (TME). They are generally regarded as a central component of both primary and metastatic tumours. They are known to profoundly

affect the behaviour of tumour and other stromal cells. CAFs (are also referred as activated fibroblasts) are reactive to stroma in TME and they both affect and get affected by cancer cells. There are conflicting studies about how exactly affect cancer progression. The majority of studies report that they actually promote tumour growth and function, while some of them show that they suppress cancer progression. One possible explanation for this contrasting situation is that CAFs do display a high amount of heterogeneity (Yang et al, 2023). The most recent method for defining CAFs include a number of factors such as cell morphology, biomarkers and mutations. They generally offer an elongated shape, have positive expression for mesenchymal markers such as vimentin and alpha-smooth muscle actin (αSMA). The mutational background of CAFs is a rather complicated manner. Some scientists do suggest they CAFs have stable genetic alterations compared to normal fibroblasts, but the answer is not totally clear for now. Since CAFs do not represent a wide array of very specific biomarkers, it is difficult to determine their exact origin. Some studies show that some cancer cells do activate normal fibroblasts through exosomal growth factor secretion. Also, various studies point out to different possible origins of CAFs such as cancer stem cells, hematopoietic stem cells, adipocytes and pericytes (Ping et al, 2021).

CAFs are also known to play a role in the progression of cancer by facilitating specific communication modes with cancer cells. For instance, CAFs can cause non-invasive cancer cells to transform into an invasive model when co-injected into mouse models. Results indicated that cancer cells that were injected with CAFs developed into faster growing tumours (Kalluri & Zeisberg, 2006).

It was also found by Guo et al. (2021) that CAFs enhance the migration and invasion of lung cancer cells when they are present in the TME. According to their findings, lung cancer cells show increased rate of wound healing on a wound healing assay when cultured with CAF condition mediums, indicating that CAFs might promote tumour migration.

Some studies also suggest that CAF population are related with the therapy resistance seen in some types of cancers (Yamamoto et al., 2022).

1.6 Aim of The Study

The project that will be described here aims to combine two areas of research. By joining microfluidics and cellular studies, it is aimed in this study to reveal the relationship between normal fibroblasts (HMFU19) and breast cancer cells (MCF-7 and MDA-MB-231) in terms of growth and migration. Key aspects of the research can be summarized as;

- Tagging stromal cells and cancer cells with different fluorescent proteins via viral transfection and antibiotic selection.
- Designing two different microfluidic chips with differing characteristics. The co-culture chip, which is a relatively standard design, will both serve as a baseline of experiments and act as a proof-of-concept device to show that multiple types of cells can be cultured on a stereo lithography produced microfluidic chip for enlengthened time.
- By using the variable width chip, which is difficult to produce using soft lithography, showing the effect of HMFU19 cells on MCF-7 and MDA-MB-231 cells with accordance to the distance between them, also accentuating the pros of 3D lithography as opposed to more conventional means of microchip production.
- Revealing the change in migratory behaviour of both MDA-MB-231, MCF-7 as well as HMFU19 cells in relation to the presence of one another in the culture environment. Performing this would also unveil the difference between these types of cells.

CHAPTER 2

MATERIALS & METHODS

2.1 Cell Line Characteristics

MCF-7 cell line is a well-established and widely used breast cancer cell line that has been established in 1973, from 69-year-old women who had breast cancer. MCF-7 is not so aggressive and non-invasive cell line which is both oestrogen receptor (ER) and progesterone receptor (PR) positive. Therefore, it is oestrogen sensitive and quite widely used in research for anti-hormone therapy. Fibroblasts from normal breast tissue might inhibit the growth of MCF-7 cells, which means strong paracrine interactions between them (Comșa, Cimpaen and Raica, 2015). MDA-MB-231 is a commonly used cell line to study late-stage breast cancer. Unlike MCF-7, MDA-MB-231 is negative for both oestrogen receptor (ER), progesterone receptor (PR) and E-cadherin. It also expresses mutant p53, which is an important tumour suppressor protein. This triple negative breast cancer cell line, contrasting to MCF-7, is both invasive and aggressive (Welsh, 2013). HMFU19 is a human mammary fibroblast cell line that is isolated and immortalized from healthy human cells (O'Hare et. Al, 2001).

2.2 Culture Conditions of MCF-7, MDA-MB-231 and HMFU19 Cells

MCF-7 and MDA-MB-231 cells were maintained in DMEM high glucose medium (Biological Industries, Israel), supplemented with 10% fetal bovine serum (FBS), 1% Penicillin-streptomycin and 1% l-glutamine solution (Biological Industries, Israel). HMFU19 cells were maintained in RPMI1640 medium supplemented with

5% fetal bovine serum (FBS), 1% penicillin-streptomycin and 1% l-glutamine solution (Biological Industries, Israel). Incubation conditions were 5% carbon dioxide and 37C degrees for all cells, provided by cellular incubator (Nüve, Türkiye).

2.3 Sub-culturing and Cell Counting

When cells reach 70 to 80% of confluency in T75 cell culture flasks, cells are passaged using the established protocols. At the first step, the used culture media on top of cells is aspirated and discarded. Then cells are washed with Phosphate Buffered Saline (PBS) (Biological Industries, Israel) solution. Afterwards, Trypsin-EDTA (Biological Industries, Israel) solution is applied on top of the cells to break surface adhesion proteins and detach cells both from each other and from the flask surface. Then the cells are incubated in cellular incubator (37 degrees Celsius, 5% carbon dioxide) for 5-7 minutes with trypsin. This causes the trypsin solution to work efficiently. Then to deactivate the trypsin solution, fresh culture media is added to flask and the solution containing detached cells is collected in a centrifuge tube. The tube is centrifuged at 180g for 3 minutes in room temperature. Then the supernatant is aspirated, the pellet is resuspended in fresh media and seeded on to a new culture flask in desired ratio depending on cell type and number.

In order to count live and dead cells in a given suspension, a Thome hemocytometer (Marienfeld, Germany) was used. A 90µL sample from the given cell suspension is taken and mixed with 10µL of Tryphan Blue dye (Strober 2015). The mixture is homogenized using a vortex. Then 10µL from this mixture is taken and placed between the hemocytometer and a glass slide. Under a light microscope, bright blue cells are counted (they are live cells dyed by Tryphan Blue). The equation given below was used to determine the number of live cells in the mixture.

Cell number/ mL= Average cell count per square x Dilution factor x 4 x 10^6.

2.4 Fluorescence Tagging Of Cells

In order to investigate them under microscope more clearly, the cells needed to be tagged with a fluorescent protein. Also, in order to differentiate stromal cells from cancer cells under microscope, they needed to be tagged in different colours. Stromal cells (544CAF and HMFU19) were tagged with a green fluorescent protein (GFP) and cancer cells (MDA-MB-231 and MCF-7) were tagged with a red fluorescent protein (RFP). To do that, the cells were seeded into two different 10cm petri dishes, in a 2 million cells/dish manner. The following day, when cells were around 50-60% confluency, corresponding vector carrying lentiviral particles were given in the cell medium to one of the two petri dishes. The amount of virus in medium was, 5ml of virus in 10ml of cell culture media with 8 µg/mL Polybrene. The next day, cell culture media was aspirated from both dishes and replaced with Puromycin (Invivogen, France) carrying media. The reason for this was to be able to eliminate the cells in the population that did not take up the insert from the virus. Since the vector does carry a puromycin resistance gene, the cells that took the insert were able to survive the exposure to puromycin, whilst non-receiving cells died. Puromycin was kept in the environment until all the cells in the control group (the dish that did not receive any virus) died off completely. Afterwards, the fluorescent emission of cells was checked under microscope. The determination of puromycin concentrations will be explained in the next section.

2.5 Determination of Lethal Puromycin Concentration

To determine the puromycin dosage that will kill all the non-resistant cells, a kill curve experiment was performed for each cell line. For each one of the three cell lines that are to be tagged (MCF-7, MDA-MB-231 and HMFU19), a 24-well-plate was set up. 5 different concentrations of puromycin solution in culture media were prepared via serial dilution. Cells were seeded on wells (except the last row, that row

was left empty to read the background luminance of corresponding puromycin solution). The seeding density was 50.000 cells/well. The day following the seeding, normal cell culture media was removed and puromycin containing media was given. Cells were kept in puromycin until all the cells in wells with the highest dose of puromycin completely died. Afterwards, an MTT assay was applied to analyze the cell viability in every well.

MTT stands for 3-(4, 5-dimethylthiazol-2-yl)-2, 5- 15 diphenyltetrazolium bromide. It is a commonly used assay to assess cell viability. Once the cells in the highest concentration of puromycin died, MTT solution was applied to all wells. The solution was prepared in 5 ml/mL MTT (Serva, Germany) with PBS and applied to each well. The plates were left in cellular incubator for 4 hours. After 4 hours, formazan crystals were formed in wells due to MTT reacting with cellular metabolites. To dissolve these crystals, 10% SDS (sodium dodecyl sulphate) solution was added to wells. After incubation, the colorimetric measurement of wells were taken via a microplate spectrophotometer (Multiskan GO; Thermo Fisher Scientific, USA) at 570nm wavelength. Cell viabilities in control group (the column without any puromycin) were taken as 100% and computed accordingly. Background noise readings of culture media or corresponding puromycin solution were also subtracted. The dosages for each cell line are given in the table below.

Table 1 Puromycin dosages used in kill curve experiment for each cell line.

	1st Dose	**2nd Dose**	**3rd Dose**	**4th Dose**	**5th Dose**
HMFU19	6 µg/ml	3 µg/ml	1.5 µg/ml	0.75 µg/ml	0.375 µg/ml
MCF-7	4 µg/ml	2 µg/ml	1 µg/ml	0.5 µg/ml	0.25 µg/ml
MDA-MB-231	5 µg/ml	2.5 µg/ml	1.25 µg/ml	0.6 µg/ml	0.3 µg/ml

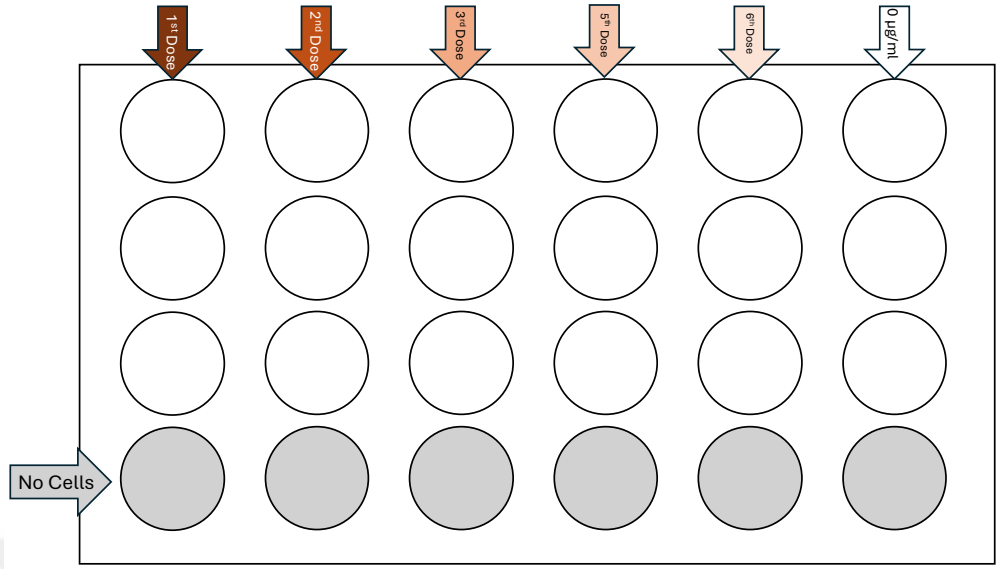

Figure 2.1 Plate layout used for puromycin kill curve experiments.

2.6 3D Printed Mold Fabrication

For each type of chip, a CAD model was prepared. Afterwards, the CAD model was sliced for 3D printing. The models were designed in CadQuery with parametric settings. Then, they were prepared for 3D printing by slicing them with Lychee Slicer. The exports of Lychee software were examined in UVTools for any mismatch.

3D printing of molds were done by using an Anycubic MONO4K 3D SLA printer with an LCD screen resolution of 35 µm. After the printing process, molds were removed from build plate, cleaned and post cured. To clean them, isopropyl alcohol (IPA) was used. The molds were first rinsed with IPA and then left in IPA for about 1 minute. The first wash was carried in a tall container filled with IPA. Then they

were washed with fresh IPA in a different container. Finally, the molds were submerged in IPA and sonicated for 5 minute and dried with pressurized air. At this point, no uncured resin was left on the molds. To finalize to procedure, post curing was applied. To do that, molds were submerged in IPA in Anycubic Wash&Cure 2.0 using UV light at 405nm. After that, molds were safe to touch and ready to be used. For the Anycubic 3D printer, an epoxy resin with 3:7 ration (3 parts Phorozen high temperature resin, mixed with 7 parts Anycubic clear raisin). A vertical printing style and 3 seconds of exposure time was used. Below is the design blueprint of the co-culture chip designed by Dr. Altuğ Özçelikkale and Barış Dedekargınoğlu.

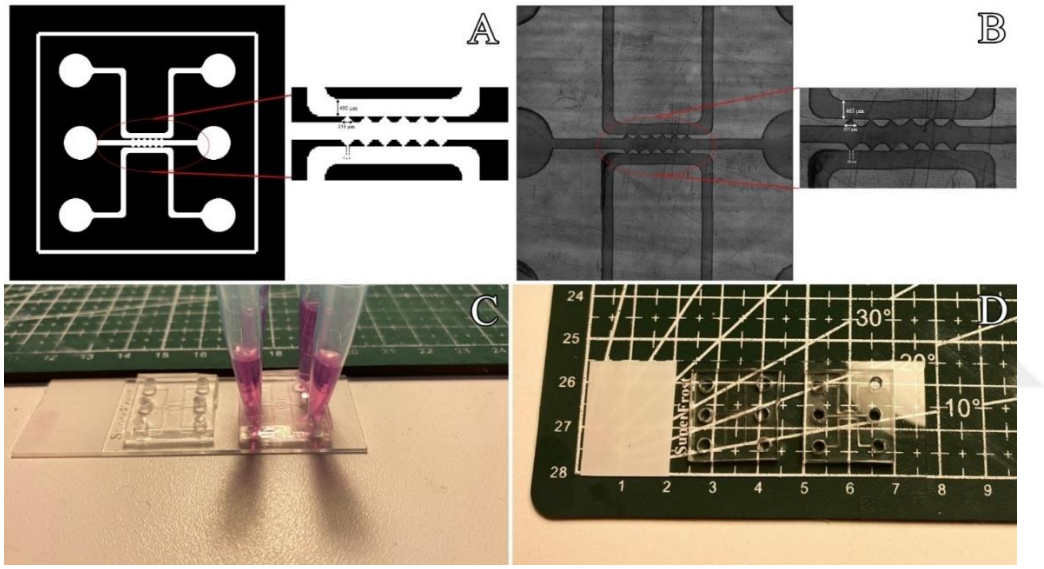

Figure 2.2 Image showing design blueprint, manufactured mold micrograph and chips in use. A) Design blueprint of co-culture chip showing initial design parameters. The designed height of channels was 220 µm. B) Microscopy image of the co-culture mold produced with measured parameters after manufacturing. The measured height of channels was 218 µm. C) A chip in use after perfused with culture media and inserted medium reservoirs. D) Photograph of a chip before perfusion, after bonding.

A different type of microchip (variable width) was also designed by Dr. Altuğ Özçelikkale and Milad Fathi allowed us to visualize the migration of cells in the presence of an internal control. Since the distance between cells was differing at

every point of the chip, the actual behaviour of cells in relation to distance to other type of cell was observed in the same chip. In addition, the 3D details on this type of chip (such as the distance in z-axis between seeding channel and collagen channel), are hard to recreate in a photo lithography, it demonstrates the advantages of stereo lithography over more conventional methods.

Below is the design blueprint of the variable width chip designed by Dr. Altuğ Özçelikkale and Milad Fathi, produced by Phrozen (Phrozen Technologies, China) 3D printer.

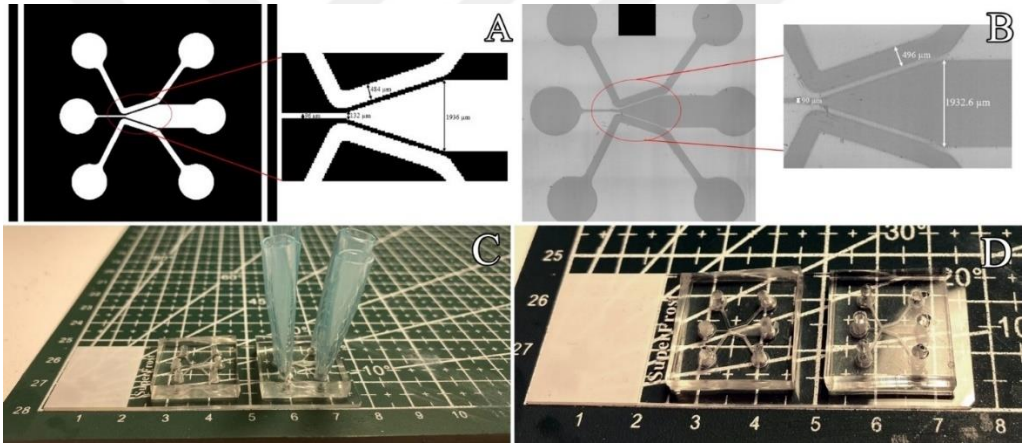

Figure 2.3 Image showing design blueprint, manufactured mold micrograph and chips in us for variable width chip. A) Design blueprint of variable width chip showing initial design parameters. The designed height of channels was 2000 µm. B) Microscopy image of the co-culture mold produced with measured parameters after manufacturing. The measured height of channels was 196 µm. C) A chip in use after perfused with culture media and inserted medium reservoirs. D) Photograph of a chip before perfusion, after bonding.

Figure 2.4 Photograph of the Anycubic 3D printer used to manufacture molds used in this experiment.

2.7 PDMS Replica Molding

To generate useful microfluidic chips from moulds, SYLGARD PDMS (SYLGARD, Germany) was used. The final mixture was prepared by mixing the silicone base with curing elastomer at a ratio of 10:1 by weight. The mixture was mixed with a spatula until it looks opaque. However, during the mixing process some bubbles were formed in the solution. To rectify this problem, the mixture was put in a vacuum chamber and exposed to suction until all the bubbles disappeared. Afterwards, the PDSM mixture was poured on to molds. Any remaining bubbles were bursted using a syringe needle. Then the PDMS was cooked at 70°C for 3 hours. Finally, the PDMS microchips were removed from moulds using a surgical scalpel. Chips are trimmed from the edges and reservoirs were opened using a biopsy punch.

2.8 Bonding of Chips To Glass Slide

In order to culture cells in a microfluidic chip, it needs to be bond to a glass slide. To achieve this goal, a Corona treater (Elveflow, France) was used. Corona treater is a device that applies a high electrical voltage to surfaces. The electrodes on the device do ionize the surrounding air and creates a localized discharge (Borok & Laboda & Bonyar, 2021). This discharge causes the surface to get activated so the chip stick to the glass. For this procedure to work, first both PDMS chips and glass slides are washed and wiped with 70% ethanol solution and wiped. Dried with compressed air and the surface that needs to be treated (surface with channels for chips) are cleaned by pasting a tape on them and peeling it. By doing that any remaining dust or other types of unwanted particles were removed from surface. Afterwards both chips (2 chips for 1 glass slide) were laid on the table, all metal surfaces were removed, and corona treatment was applied to them for about 45 seconds, with multiple passes.

Finally, the bound chips were left to cook in 100°C in an oven or on a hot plate overnight with a weight on top to ensure perfect binding.

2.9 Collagen Coating of Chips

The channels of microchip needed to be coated with a thin layer of collagen to promote cellular attachment. To achieve this, first channels of chips were washed with water and 70% ethanol then dried with compressed air and heat. In the next step, the chips were placed in laminar flow hood and sterilized with UV light for sterilization. Then a 0.05mg/ml collagen solution was prepared by using a type I rat tail collagen (Corning, United States). The solution was given to channels by using a micropipette from reservoirs. Once all the channels are filled with collagen solution, the chips were placed in cellular incubator at 37°C for collagen to polymerize. After 45 minutes, the procedure was applied for a second time to ensure contact of solution to every point in channel. Chips were placed in incubator once again and incubated for 45 minutes. Then the channels were washed with autoclaved distilled water. Finally, the chips were left to dry out in incubator for 2-3 days.

2.10 Cellular Loading and Migration Assay on Microchips

Once the chips were coated with collagen and dried out, they were ready to be used in cellular experiments. At first, the middle channel needed to be filled with a collagen gel to create a medium that separates cancer cells from stromal cells. To do that, a 6 mg/ml collagen solution was prepared and given to the middle channel via reservoir opening until the channel is filled. Any remaining empty space in reservoir area was topped of with this collagen gel too. Once the channel is filled, the chips were placed in 37°C incubator for collagen polymerization for 45 minutes. Then cells

were trypsinized and counted. In opposing channels, different types of cells (each channel was containing a different type of cell) were seeded by giving a 1*10^6 cells/ml density by giving a cell suspension from reservoirs. Cells were left to settle in the incubator for about 1 hour. After that, medium reservoirs were installed to cell chambers and filled with culture media. The reservoirs were made by cutting micropipette tips at the size of cell chamber inserts.

2.11 Examination Of Chips Under Fluorescent Microscope

After chips are loaded with cells, they were cultured for 1 week. The images were taken by a Nikon Ti2 fluorescent microscope (Nikon, Japan). The images are taken with 4X magnification and 465nm for GFP signal, 550nm for RFP signal.

2.12 Analysing the Migration and Confluence Index of Cells

After the images are taken, RFP and GFP signals were analysed using Fiji software. The signals are cleaned from background noise via Fiji's segmentation plug-in. Then the segmented images were analysed using MATLAB software. The number of particles (fluorescent emitting cells) in the middle channel filled with collagen was counted and position of each signal was plotted according to a determined reference point. By performing this analysis for images taken in different days, the average migration distance of cells was determined. By doing this the migratory behaviour of cells according to the culturing configuration (e.g. MDA-MB-231 alone vs MDA-MB-231 and HMFU in opposing channel).

CHAPTER 3

RESULTS

The major aim of this study was to investigate and demonstrate the effects of stromal cells present in culture environment on the migratory behaviour of cancer cells. To examine the situation, MDF-7 and MDA-MB-231 cells were cultured both in the presence and absence of fibroblasts in the environment. These conditions were fulfilled by seeding cells on microfluidic chips in different configurations. By comparing co-cultured and monocultured chips, the effects of fibroblasts on cancer cells, if any, would be demonstrated in terms of migratory behaviour.

In order to track the migration of cancer cells on the microfluidic chip needed to be tagged with different fluorescents. Cancer cells (MDA-MB-231 and MCF-7) tagged with RFP and stromal cells (HMFU19) tagged with GFP vectors. To eliminate the population of cells that did not express the vector, puromycin selection was performed. Since the vector was carrying a resistance to puromycin gene, the cells that did not uptake and express the vector did not survive. To find the lethal dosage of puromycin for MCF-7, MDA-MB and HMFU19 cells, a kill curve experiment was performed for each line. Below are the results of these experiments.

3.1 Puromycin Kill Curve

To eliminate cells that do not express the vector, a puromycin selection was required. To perform the selection with proper puromycin doses, kill curve experiments needed to be performed.

Below are the results of puromycin kill curve experiment done with HMFU19 cell line. According to this graph, 0.375 µg/ml was chosen as the lethal dose of puromycin and used.

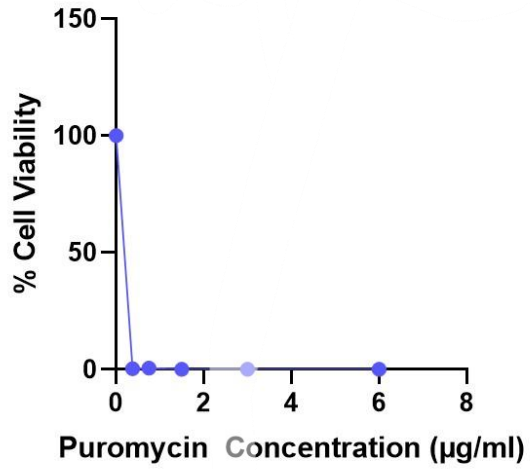

Figure 3.1 Dose response curve of puromycin on HMFU19 cell line. All the doses tested on HMFU19 cells did result in almost complete elimination of living cell population.

Kill curve results done with MDA-MB-231 cell line are listed below. According to this graph, 1.75 µg/ml was chosen as the lethal dose of puromycin and used.

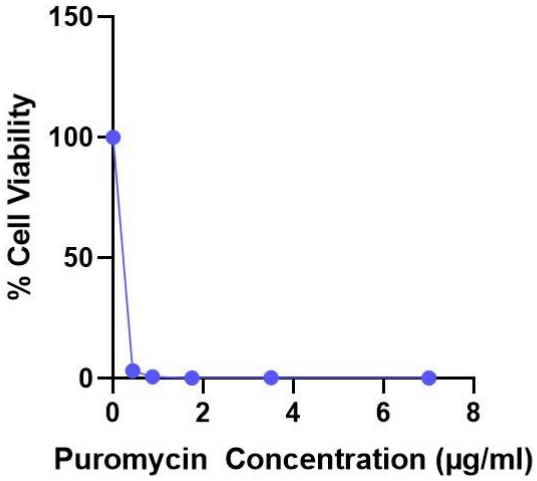

Figure 3.2 Dose response curve of puromycin on MDA-MB-231 cell line. All the doses tested on MDA-MB-231 did result in significant decrease in living cell population.

Below are the results of kill curve experiment done with MCF-7 cell line. According to this graph, 1 µg/ml was chosen as the lethal dose of puromycin and used.

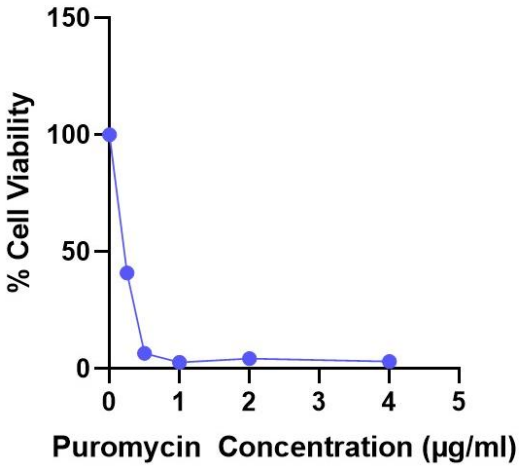

Figure 3.3 Dose response curve of puromycin on MCF-7 cell line. Doses tested on MCF-7 cells did result in significant decrease in living cell population. However, a small portion of cells did survive in 0.5 µg/ml, 1 µg/ml and 2 µg/ml concentrations.

3.2 RFP and GFP Emission Confirmation of Cell Lines

Below are the fluorescent microscope images of corresponding cell lines that are taken in both with bright field an under an excitation laser. The wavelength for GFP tag was 465nm and 550nm for RFP tag. The images show that RFP and GFP inserts were taken up by cells and expressed since they both give emissions under suitable excitation lasers.

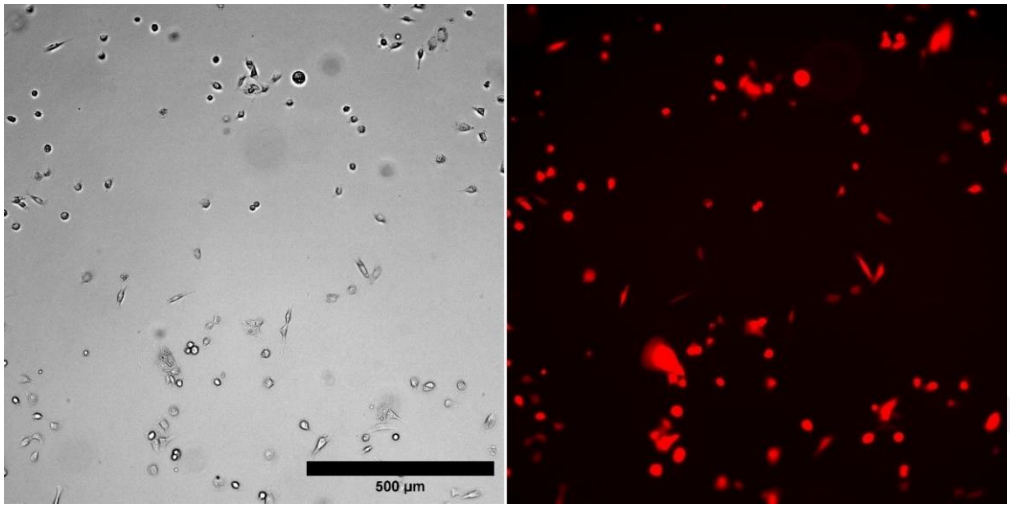

Figure 3.4 Bright field (left) and RFP (right) images of MDA-MB-231 cells after tagging. Images are taken at 10X magnification.

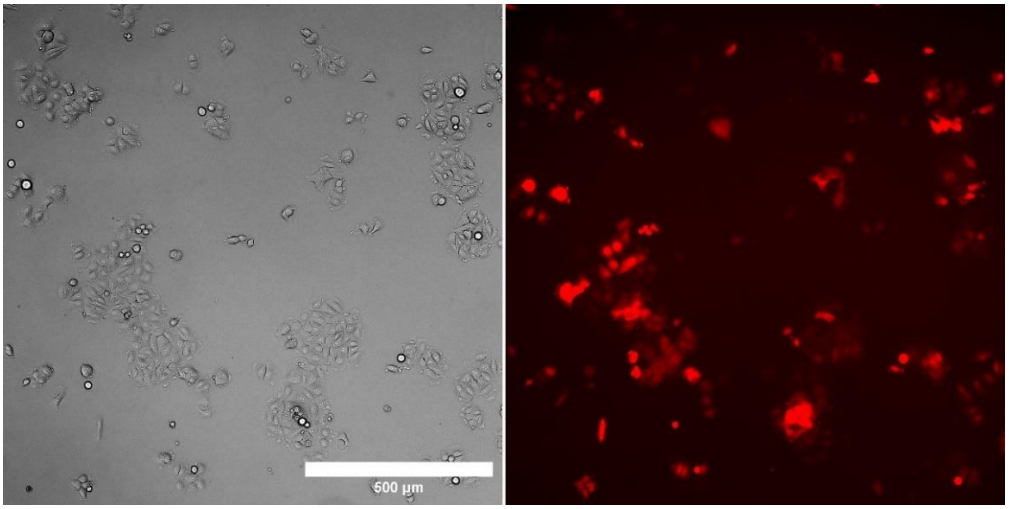

Figure 3.5 Bright field (left) and RFP (right) images of MCF-7 cells after tagging. Images are taken at 10X magnification.

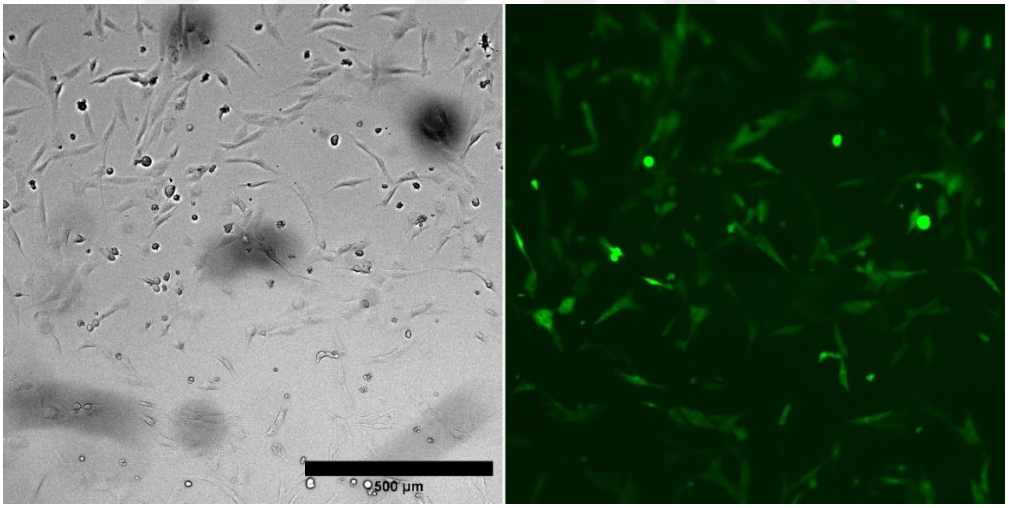

Figure 3.6 Bright field (left) and GFP (right) images of HMFU19 cells after tagging. Images are taken at 10X magnification.

3.3 Constant Width Co-Culture Microchip Migration Assay Results for Cancer Cells

Below are the fluorescent microscopy images of microchip migration assay done with MDA-MB-231 and HMFU19 cells. Different cell lines were seeded on opposing channels of the chip at 1 million cells/ml density. The middle channel was filled with 6 mg/ml collagen gel. The images were taken at 4X magnification.

According to the microchip assays and their analysis, MDA-MB-231 cells do not display a significant change in their migratory behaviour regardless of the presence of HMFU19 cells in the opposing channel. Small changes seen in control vs co-culture conditions did not show any significance according to the t-test performed. However, an interesting phenomenon was displayed by MDA-MB-231 cells that was not observed for MCF-7 cells. As, shown in the microscope images below, the collagen gel in the middle channel was either degraded or pushed away from the walls by MDA-MB-231 cells. This might be interpreted that MDA-MB-231 cells do perform a more significant extracellular matrix (ECM) remodelling when compared to MCF-7 cells.

In contrast to MDA-MB-231 cells, MCF-7 cells do display a significant change in migratory behaviour in the presence of HMFU19 cells by increasing their migration potential.

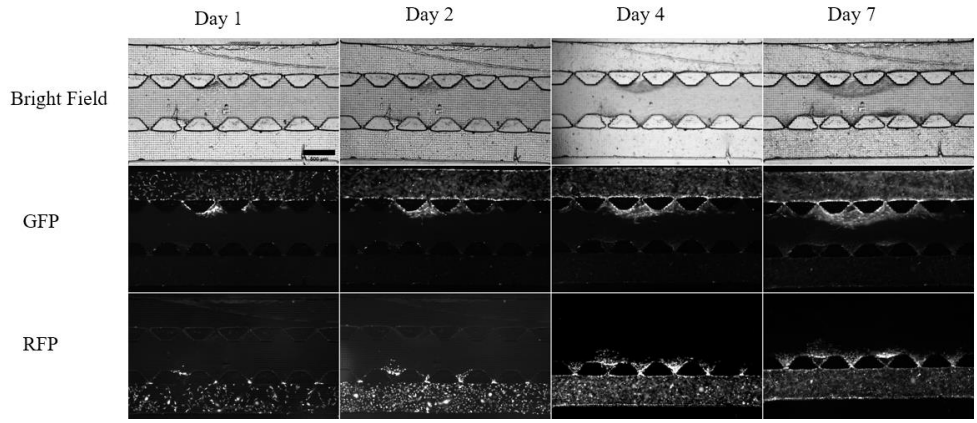

Figure 3.7 Fluorescent microscopy images of chip loaded with MDA-MB-231 (bottom channel) and HMFU19 (top). Images are taken at 4X magnification and scale bar is 500 µm.

The segmentation process allows a machine learning algorithm to process the image to separate background from cells that give off signal. These results demonstrate the migration pattern of MDA-MB-231 cells when cultured with HMFU19 cells in the opposing channel. It can be seen theMDA-MB-231 cells both fill up the channel that they were initially seeded to and migrate towards the opposite direction, through the collagen gel.

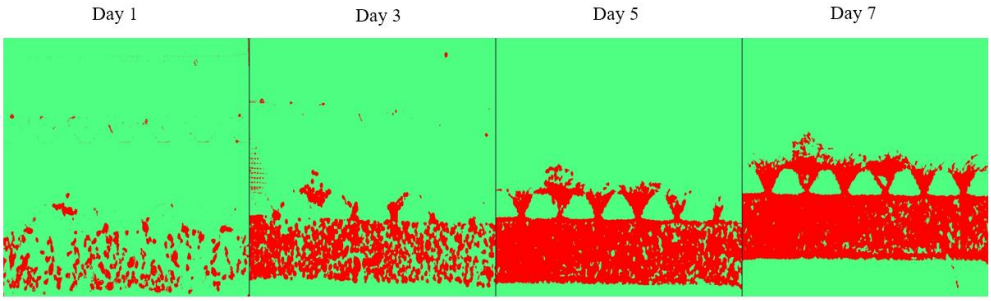

Figure 3.8 Migration pattern of MDA-MB-231 cells on chip displayed at Figure 3.7, after the signals were analysed and separated from backgrounds via Fiji's Weka Segmentation plugin. Cells are marked with red, displaying growth and migration behaviour when cultured with HMFU19 cells in the opposing channel.

The segmentation analysis shown in Figure 3.8 is done for every chip in order to allow MATLAB to process the images.

To compute the confluence based on location, a MATLAB script was used. To perform this analysis, the code scans the entire image by dividing it to lines parallel to x-axis. It counts the entire line and processes any pixel that gives a fluorescent signal as 1, while counts non-fluorescing pixels as 0. By dividing the sum of these values to the entire length of the pixel line, a confluence ratio is obtained and then plotted with respect to location. Below are the results of this calculation for first and seventh days of chip shown in Figure 3.7.

Afterwards, to compute the index that we defined as “migration index”, a reference point on the image was selected. By dividing the total fluorescent are beyond the reference point to the fluorescent area below, a “migration index” is calculated.

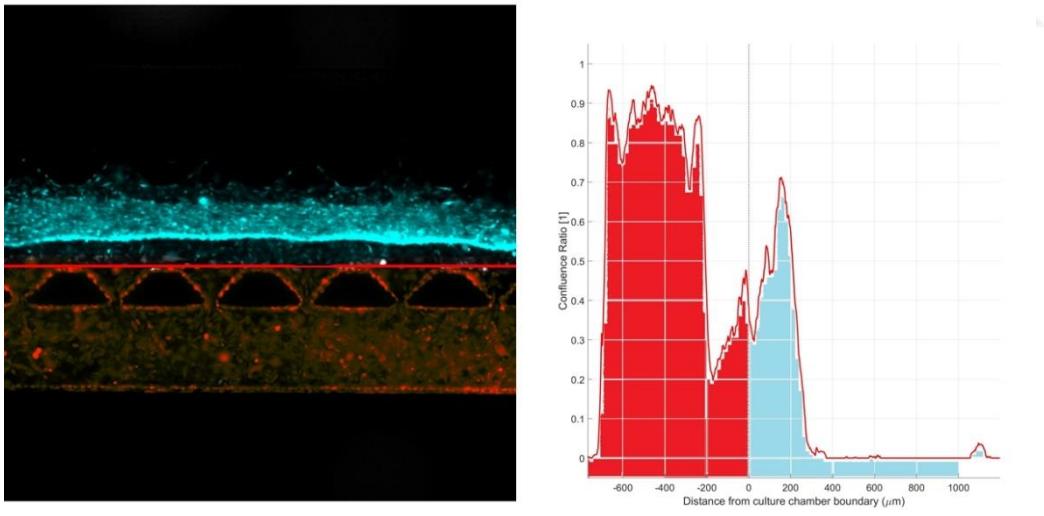

Figure 3.9 Schematic representation of migration index. Red line represents the reference point. Total fluorescence emitting area in red is S_1. Total fluorescence emitting area in blue is S_2. S_2/S_1 gives the migration index (images shown here are just given as examples, not actual results).

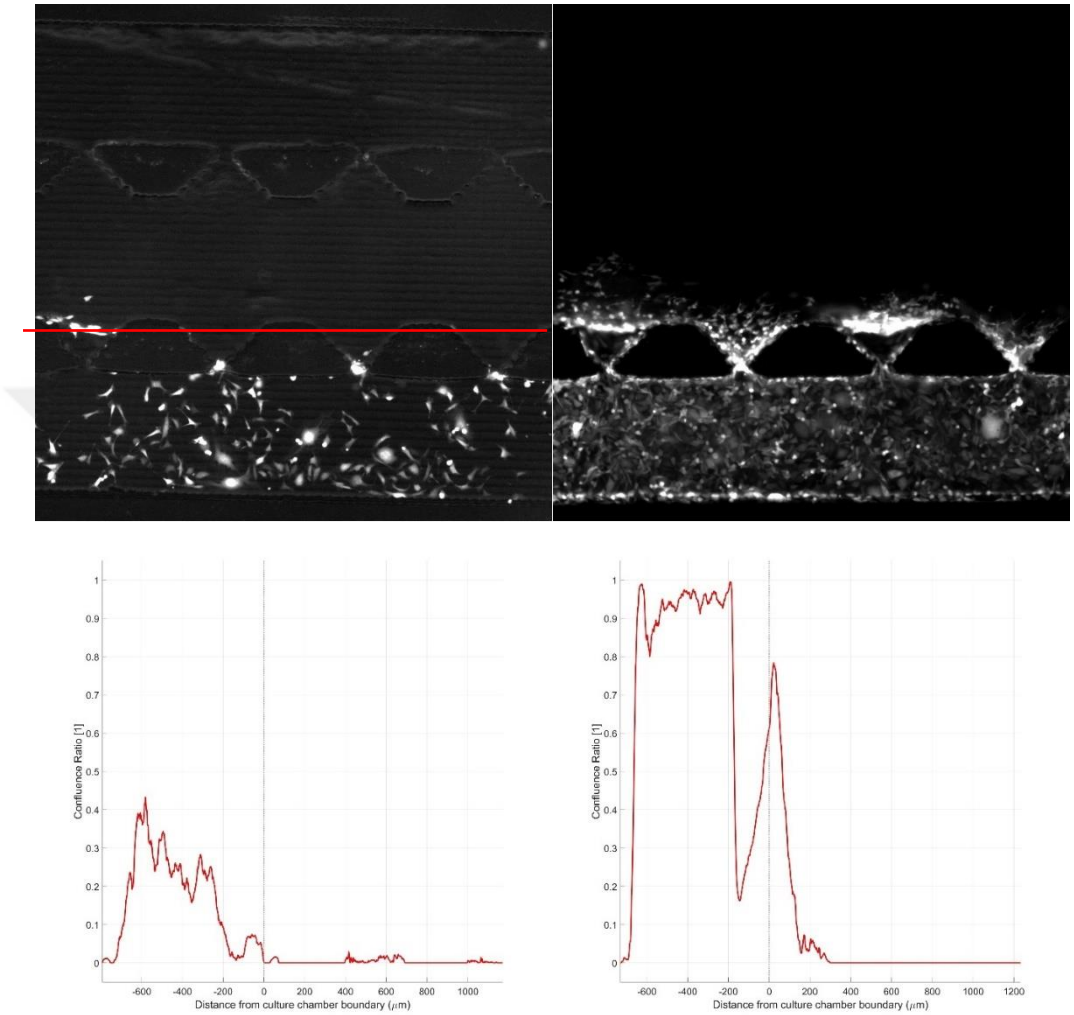

Figure 3.10 The confluence ratio graphs of chip shown in figure 3.7, loaded with MDA-MB-231 (lower channel) and HMFU19 (not shown here, upper channel) cells. Images on the top row represent the RFP images and images on the bottom row represent the confluence ration. X-axis on the graphs correspond to y-position on the actual microscopy image. Point 0 on graphs is marked with red line on microscopy image.

As it can be seen in the microscopy images, this analysis confirms that throughout the culture time, MDA-MB-231 cells both grow and migrate towards the opposing channel. In the graph drawn from seventh day image, it can be seen that many cells

crossed the border point, towards to opposing channel whereas in the graph drawn from first day image there are almost no cells beyond the border point.

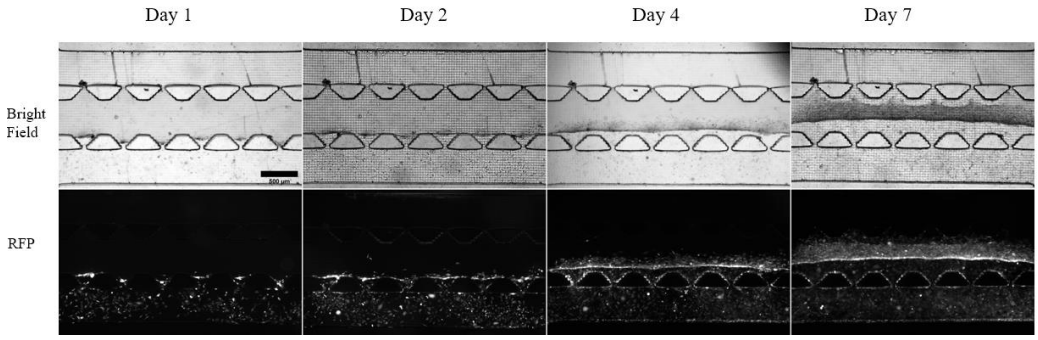

Figure 3.11 Fluorescent microscopy images of chip loaded with MDA-MB-231 (bottom channel) and blank medium (top). Images are taken at 4X magnification and scale bar is 500 µm.

The same confluence ratio calculation was also applied to the chip seen on figure 3.10 which was seeded only with MDA-MB-231 cells. Below are the results of the analysis.

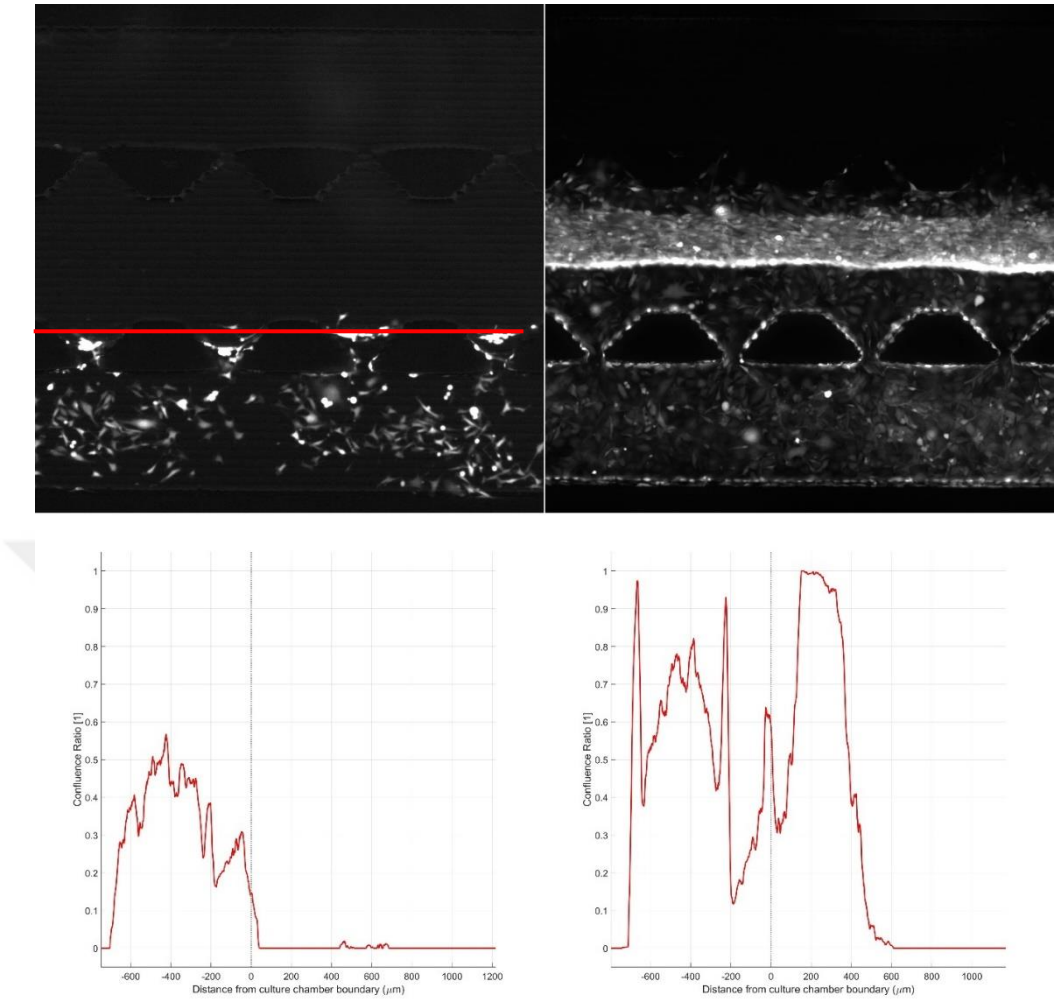

Figure 3.12 The confluence ratio graphs of chip shown in figure 3.11, loaded with MDA-MB-231 (lower channel) and blank media (not shown here, upper channel). Images on the top row represent the RFP images and images on the bottom row represent the confluence ration. X-axis on the graphs correspond to y-position on the actual microscopy image. Point 0 on graphs is marked with red line on microscopy image.

As it can be seen in the microscopy images, this analysis confirms that throughout the culture time, MDA-MB-231 cells both grow and migrate towards the opposing channel. In the graph drawn from seventh day image, it can be seen that many cells crossed the border point, towards to opposing channel whereas in the graph drawn from first day image there are almost no cells beyond the border point.

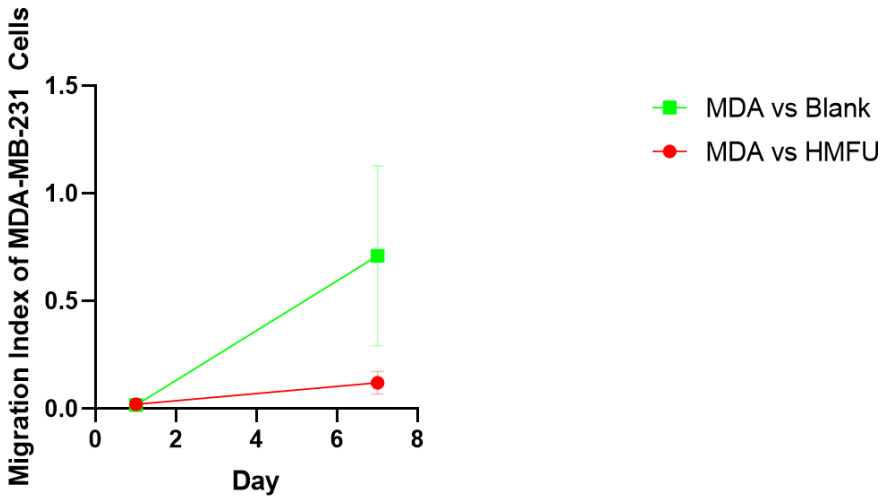

Figure 3.13 Graph of the change in migration index of MDA-MB-231 cells in the presence and absence of HMFU19 cells in the opposing channel.

According to the analysis done with the chips above, with MDA-MB-231 cells and HMFU19 cells, in 7 days, the migration index of the MDA-MB-231 cells appear to be higher when cultured without HMFU19 cells in the opposing channel. However, a t-test applied between these two groups result in a non-significant output. On the other hand, a linear regression test shows that the slopes of these two lines are significantly different. This result can be interpreted as the final point that the MDA-MB-231 cells migrate to do not change in the presence or absence of HMFU19 cells. But their migration rate differs, increasing in the presence of HMFU19.

A similar situation persists when chips were cultured for 6 days instead of 7 and analysed accordingly. In both comparisons done (either day 1 vs day 7 or day 1 vs day 6), migration index of MDA-MB-231 seems to be a little bit higher when cultured with HMFU19 cells, however this difference is not significant statistically, in both t-test and linear regression.

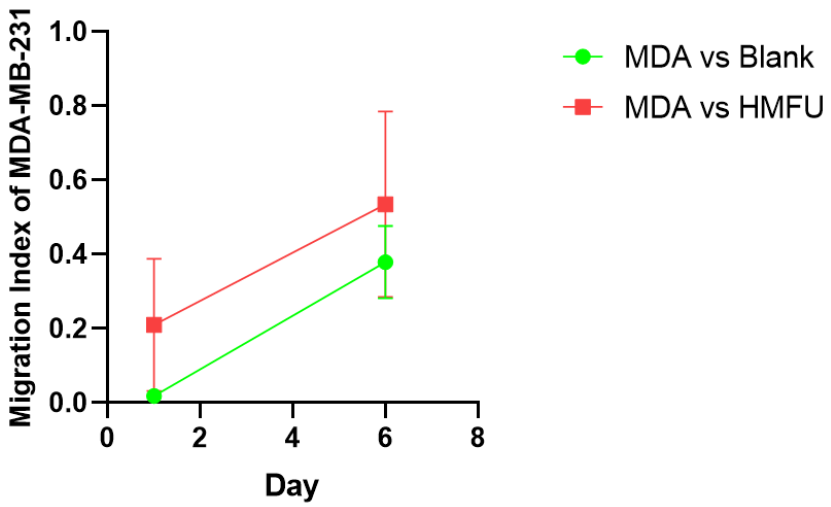

Figure 3.14 Graph of the change in migration index of MDA-MB-231 cells in the presence and absence of HMFU19 cells in the opposing channel.

However, in both experiments done with MDA-MB-231 cells, a collagen separation from the walls when MDA-MB-231 cells reach the gel was observed. In order to assure that this is not an experimental or technical problem, a set of chips were loaded with only MDA-MB-231 cells and observed. To ensure that this phenomenon is indeed caused by cellular activity rather than a technical issue, cells were loaded to different channels on different chips.

However, in all chips loaded with MDA-MB-231 cells, the collagen separation from the walls was observed. Collagen gel either gets pushed away or biochemically broken down by MDA-MB-231 cells. MDA-MB-231 cells confidently infiltrate the empty space left behind by separated collagen gel.

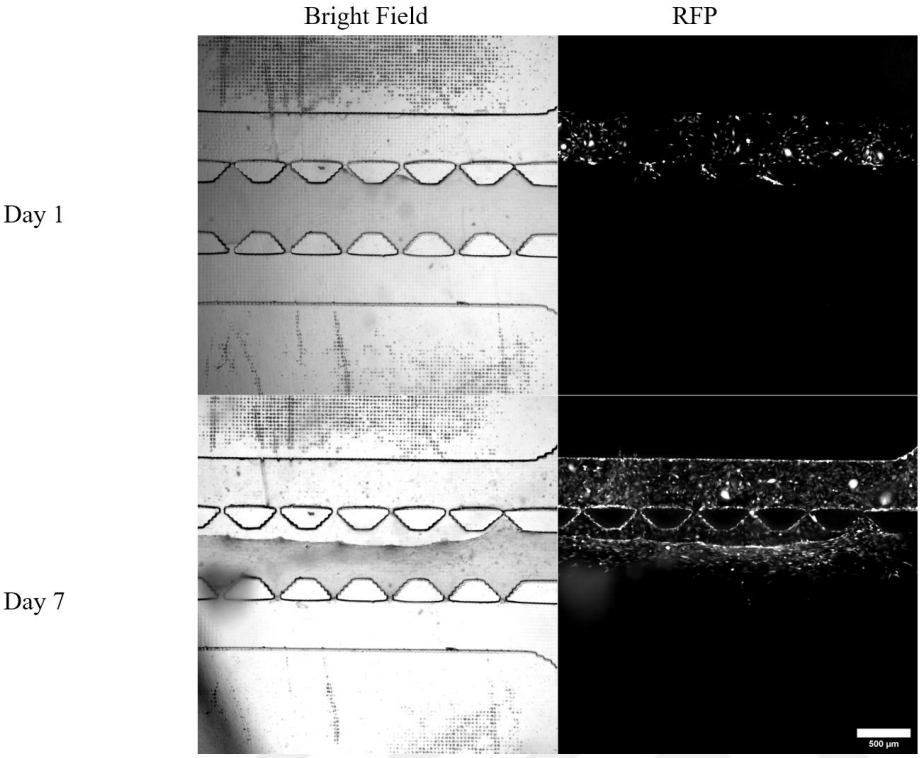

Figure 3.15 Fluorescent microscopy images of chip loaded with MDA-MB-231 (top channel) and blank media (bottom channel). Bright field image clearly shows the separated collagen gel at day 7. The line that separates the collagen from channel walls overlaps perfectly with RFP signal from cells. Images are taken at 4X magnification and scale bar is 500 µm.

To observe the differences between behaviours of MDA-MB231 and MCF-7 cells, the experiments described before were repeated with using MCF-7 and HMFU19 cells. Chips were loaded with either in a co-culture (2 different cell types in opposing channels) or in a mono-culture (a single type of cell opposing blank culture media) configuration. Below are the results of microchip assays done with MCF-7 and HMFU19 cells.

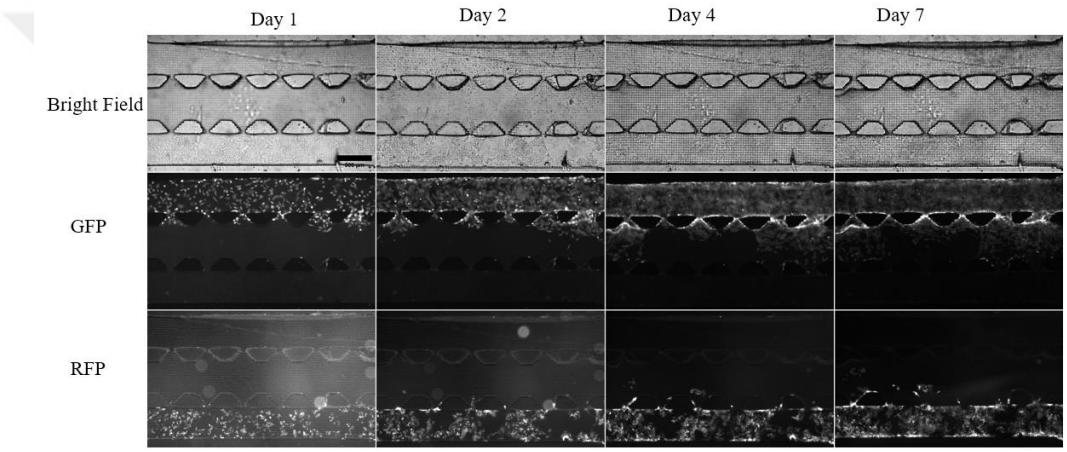

Figure 3.16 Fluorescent microscopy images of chip loaded with MCF-7 (bottom channel) and HMFU19 (top channel). Images are taken at 4X magnification and scale bar is 500 µm.

According to these results, MCF-7 cells display a lower tendency to migrate towards the middle channel when compared to MDA-MB-231 when cultured with HMFU19 cells, as expected since MDA-MB-231 is a more aggressive type of breast cancer.

Below are the results of confluence ration calculation of chip shown in Figure 3.16, as described previously.

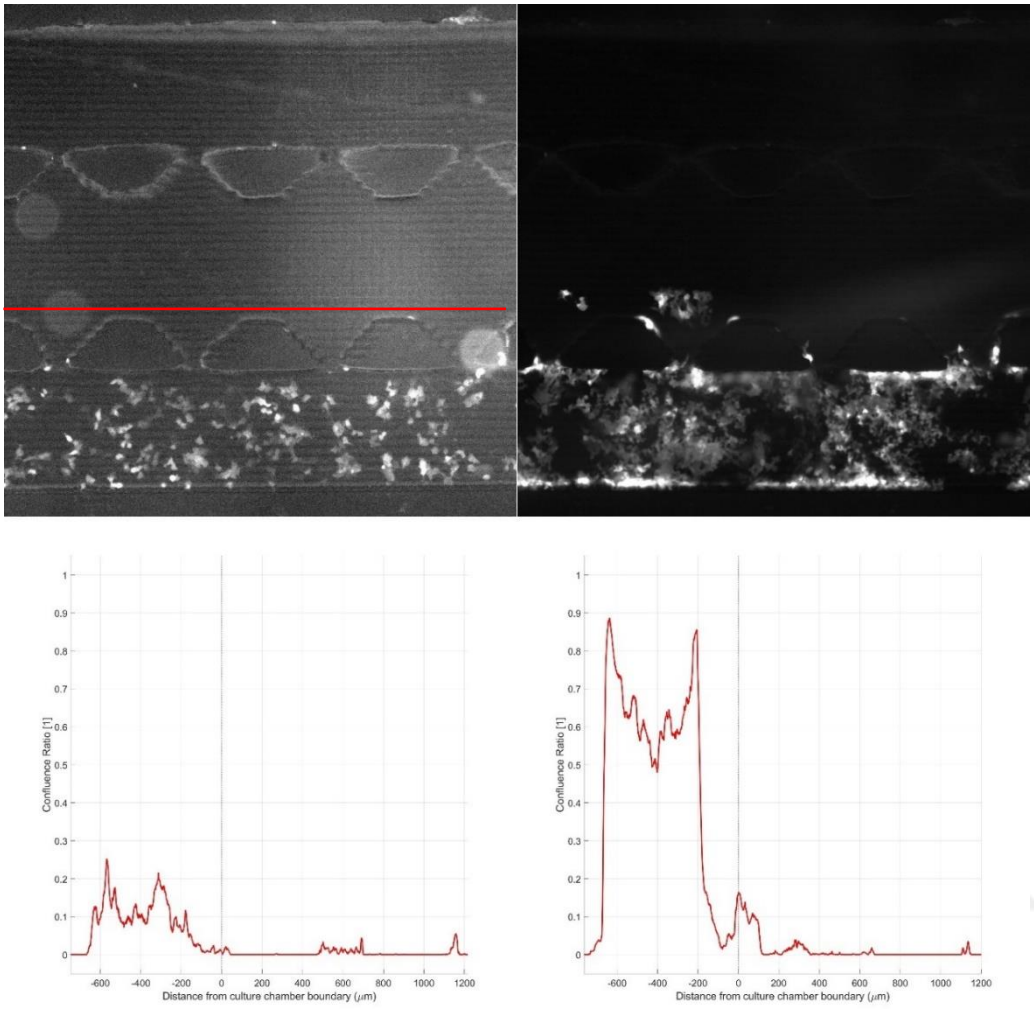

Figure 3.17 The confluence ratio of MCF-7 on chip shown in figure 3.16, loaded with MCF-7 (lower channel) and HMFU19 cells (not shown here, upper channel) cells. Images on the top row represent the RFP images and images on the bottom row represent the confluence ration. X-axis on the graphs correspond to y-position on the actual microscopy image. Point 0 on graphs is marked with red line on microscopy image.

Microscopy images and confluence ratio calculations show that throughout the culture time MCF-7 cells do grow but a few of them actually cross past the border point and migrate towards the opposing direction.

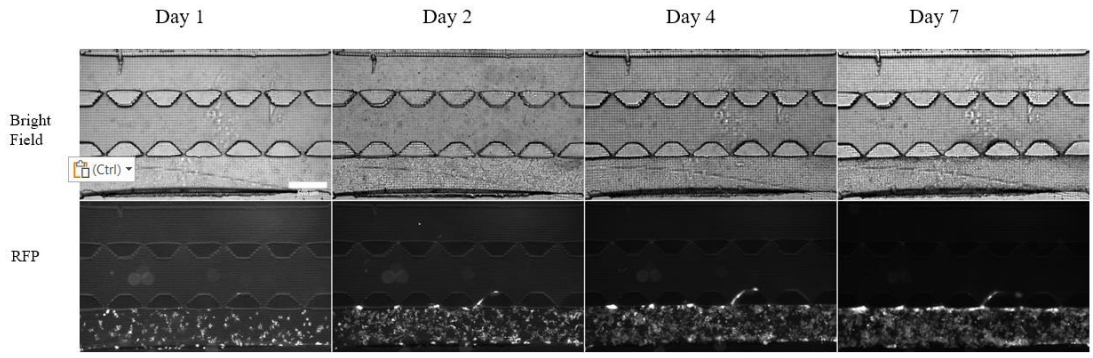

Figure 3.18 Fluorescent microscopy images of chip loaded with MCF-7 (bottom channel) and blank media (top channel). Images are taken at 4X magnification and scale bar is 500 µm.

These analysis results display that even though the migration tendency of MCF-7 cells was not very high in the co-culture setting, it is even less prominent when MCF-7 cells cultured without any type of cell. The confluence ratio analysis of chip seen on Figure 3.19 can be found in the next figure.

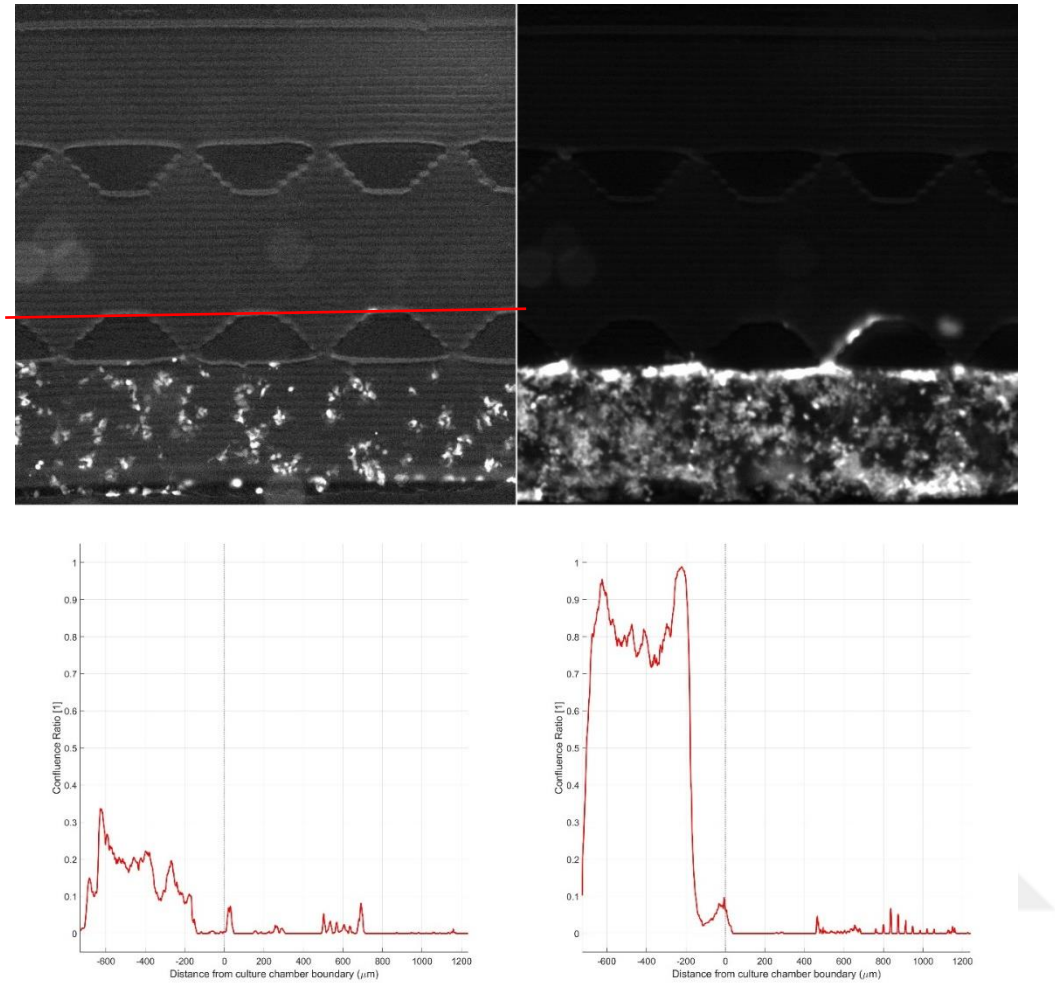

Figure 3.19 The confluence ratio of MCF-7 on chip shown in figure 3.18, loaded with MCF-7 (lower channel) and blank media (not shown here, upper channel). Images on the top row represent the RFP images and images on the bottom row represent the confluence ration. X-axis on the graphs correspond to y-position on the actual microscopy image. Point 0 on graphs is marked with red line on microscopy image.

From the confluence ratio analysis of MCF-7 in co-culture and mono-culture conditions, it can be seen that MCF-7 does not display a strong migratory behaviour in either single or co-culture condition. However, in Figure 3.18 there are some cells passed the border point and migrated towards the middle channel. However, in

Figure 3.21 almost no cells passed the border point. From these results it can be said that HMFU19 cells affect the migratory behaviour of MCF-7 cells, even though the effect is quite minimal.

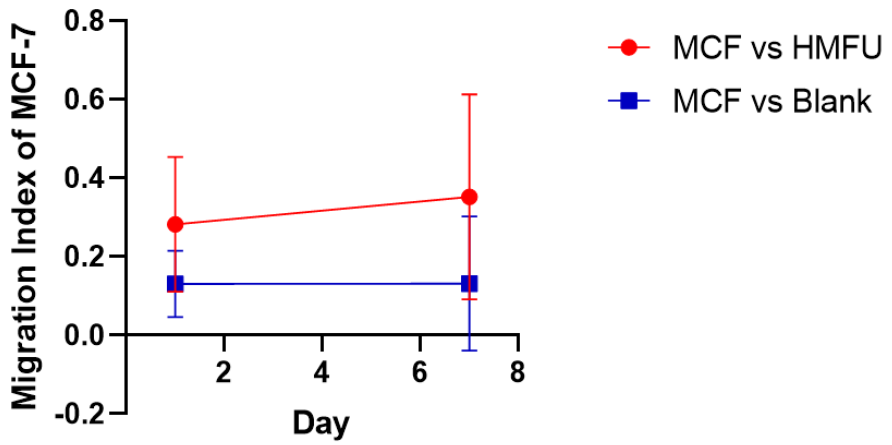

Figure 3.20 Graph of the change in migration index of MCF-7 cells in the presence and absence of HMFU19 cells in the opposing channel.

According to the analysis done with the chips above, with MCF-7 cells and HMFU19 cells, in 7 days, the migration index of the MCF-7 cells appear to be higher when cultured with HMFU19 cells in the opposing channel. Statistically this result is significant when a t-test is applied. But in contrast to the MDA-MB-231 configuration, a linear regression analysis shows that the slopes are not significantly different. This can mean that the migration rate of MCF-7 cells is independent from the presence of HMFU19 whereas the total migration is affected by fibroblast's presence.

3.4 Constant Width Co-Culture Microchip Migration Assay Results for HMFU19 Cells

During the experiments, HMFU19 cells were used as a stromal cell to investigate their effect on the migration of breast cancer cells. However, it was also observed that HMFU19 cells themselves also migrate towards the opposite channel during the culture time. Therefore, the same analysis done for cancer cells were also applied to HMFU19 cells. Below are the results.

These analysis results demonstrate that HMFU19 cells display a rather strong migration tendency in the presence of MDA-MB-231 cells. The confluence ratio calculation of HMFU19 cells in this chip will be shown in the next figure.

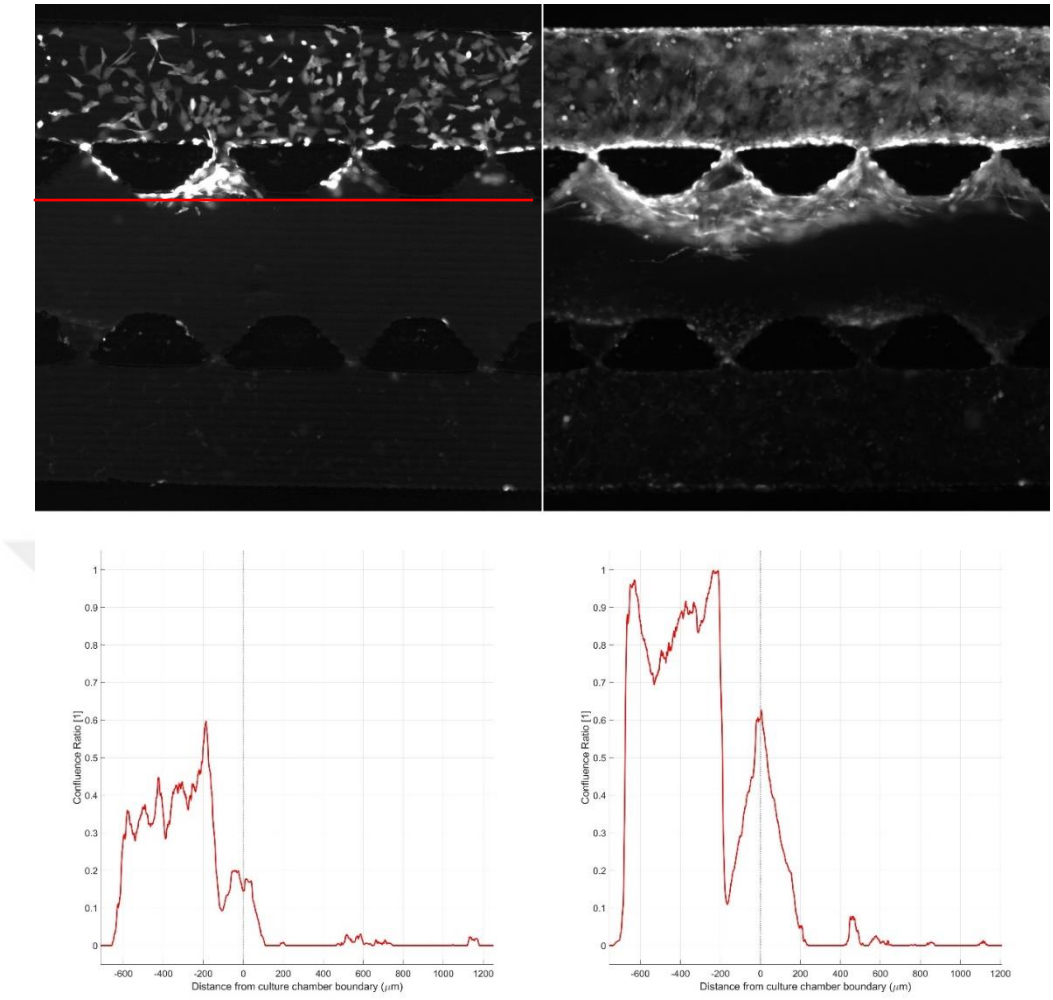

Figure 3.21 The confluence ratio of HMFU19 on chip shown in figure 3.7, loaded with MDA-MB-231 (lower channel, not shown here) and HMFU19 (upper channel). Images on the top row represent the GFP images and images on the bottom row represent the confluence ratios. X-axis on the graphs correspond to y-position on the actual microscopy image. Point 0 on graphs is marked with red line on microscopy image.

The confluence ratio calculations of HMFU19 cells show that they display a rather prominent migration tendency towards the opposing channel when cultured with MDA-MB-231 cells. However, to understand the difference between the effects of

MDA-MB-231 and MCF-7 cells on HMFU19 cells, the same analysis was conducted with MCF-7 cells too. Below are the results.

These results show that HMFU cells also display a strong migratory tendency in the presence of MCF-7 cells. The confluence ratio results done for HMFU19 cells on this co-culture chip with MCF-7 cells can be found in the next figure.

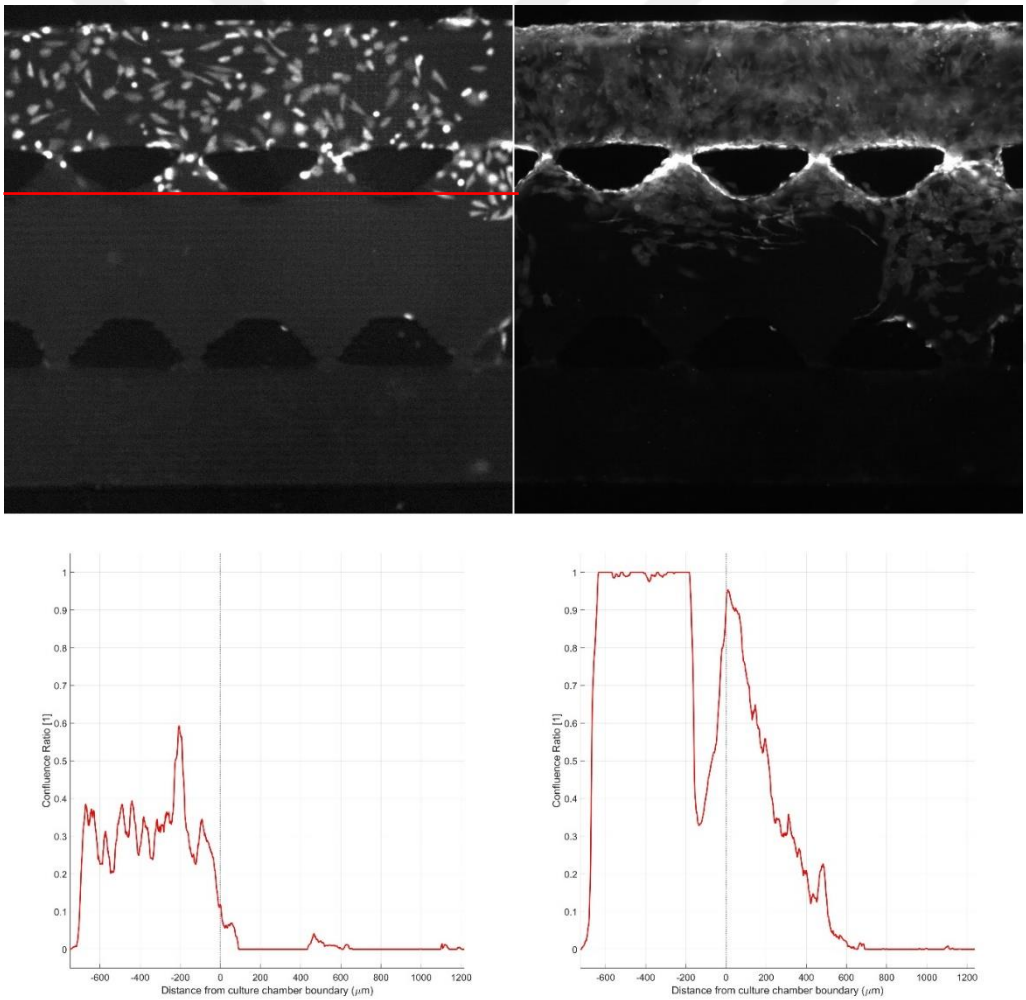

Figure 3.22 The confluence ratio of HMFU19 on chip shown in figure 3.16, loaded with MCF-7 (lower channel, not shown here) and HMFU19 (upper channel). Images

on the top row represent the GFP images and images on the bottom row represent the confluence ratios. X-axis on the graphs correspond to y-position on the actual microscopy image. Point 0 on graphs is marked with red line on microscopy image.

The confluence ratio calculations of HMFU19 cells on chip, when cultured with MCF-7 cells in the opposing channel, show that HMFU19 cells show both growth and migration tendencies.

To demonstrate the difference of HMFU19 behaviours in co-culture and mono-culture conditions, previously described experiments and analyses done with HMFU19 loaded chips without the presence of any other cell type. Below are the microscopy images of a chip loaded only with HMFU19 cells.

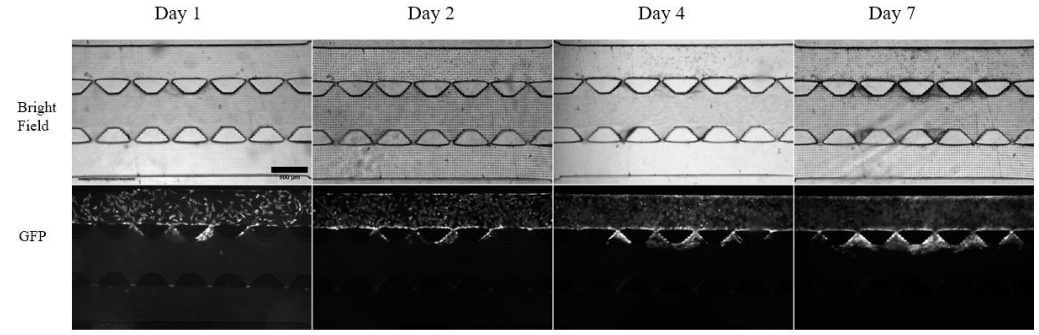

Figure 3.23 Fluorescent microscopy images of chip loaded with HMFU19 cells (top channel) and blank media (bottom channel). Images are taken at 4X magnification and scale bar is 500 μm.

From these segmentation results, it can be qualitatively argued that HMFU19 cells do not display a strong migratory behaviour when they are cultured alone, when compared to co-culture conditions where a type of breast cancer cell is present in the opposing channel.

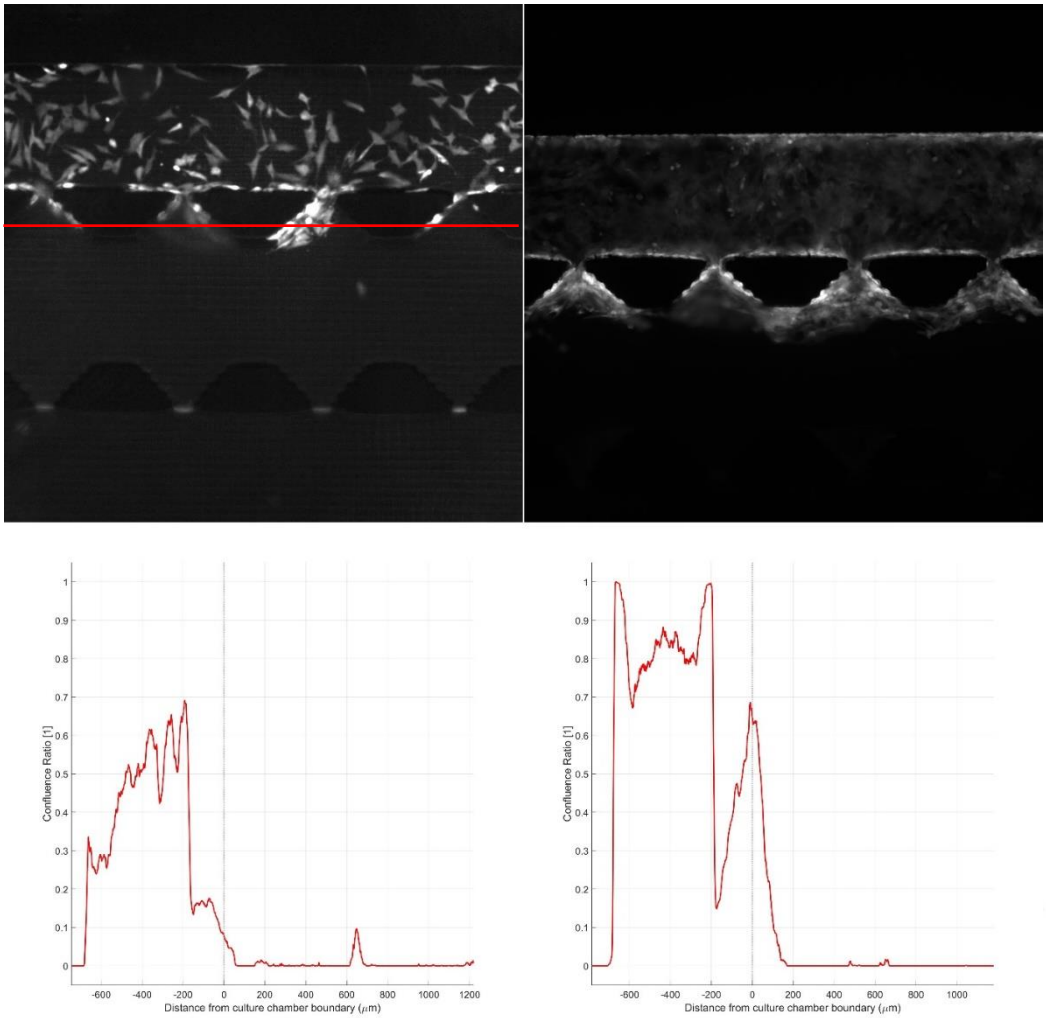

Figure 3.24 The confluence ratio of HMFU19 on chip shown in figure 3.23, loaded with HMFU19 (upper channel) and blank media (lower channel, not shown here). Images on the top row represent the GFP images and images on the bottom row represent the confluence ratios. X-axis on the graphs correspond to y-position on the actual microscopy image. Point 0 on graphs is marked with red line on microscopy image.

Confluence ratio calculations done on HMFU19 cells with no other cell type present in the environment, show that HMFU19 cells, when cultured alone do not show a very prominent migration tendency towards the opposing channel.

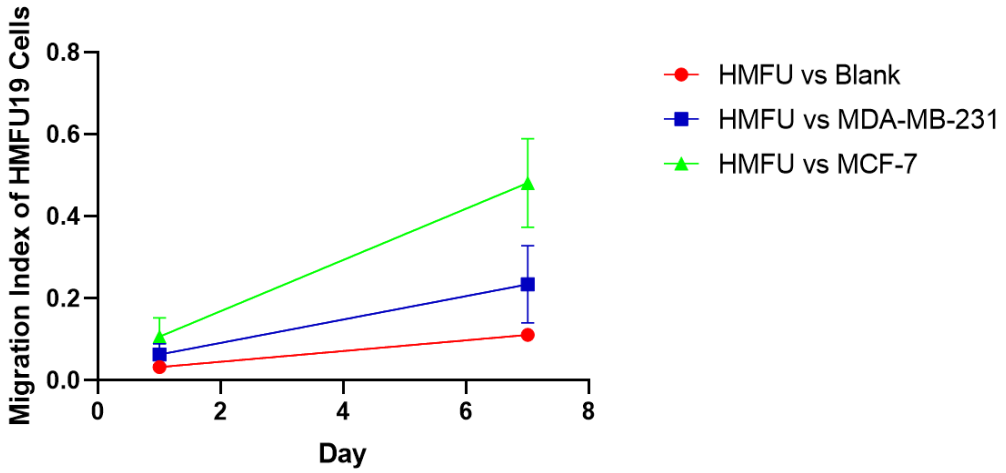

Figure 3.25 The graph showing the change in the migration index of HMFU19 cells in the presence of cancer cells (MCF-7 and MDA-MB-231) and in mono-culture (no other cell type present) condition. X-axis is the day in culture, showing the change in migration index as a function of time.

The graph on Figure 3.4.8 shows that the migratory behaviour of HMFU cells increase in the presence of a cancer cell (more so when cultured with MCF-7). However, according to a one-way ANOVA test done on these results, the difference between groups is not significant. But a linear regression analysis demonstrates that the slopes of the lines are sufficiently different from one another. Again, this result can be interpreted as the speed of migration tightly depends on co-culture conditions whereas the migration tendency as general do not depend on it.

Despite all the effort to standardize the microchip assays, there are some inescapable variation points between chips and cells in different sets of experiments. For instance, even though the molds used are the same, from time to time they display wear and tear artefacts from time to time. Moreover, passage number of cells would be different due to time passed between different experiments.

To rectify these problems, a chip with a middle channel that is varying in width was used. The change in distance between different cell line was acting like an internal control of the chip, allowing for normalization inside the cell. In addition, this chip

design was containing traits that are not easy to produce with conventional methods of microfluidic chip mold manufacturing, displaying the power of stereo lithography.

3.5 Variable Width Microchip Migration Assay Results for MCF-7 Cells

Below are the fluorescent microscopy images of variable width microchip assay done with MCF-7 and HMFU19 cells. The wedge-like area between seeding channels was filled with 6mg/ml collagen and the rest of the assay was carried out in the same approach as co-culture assays, described previously.

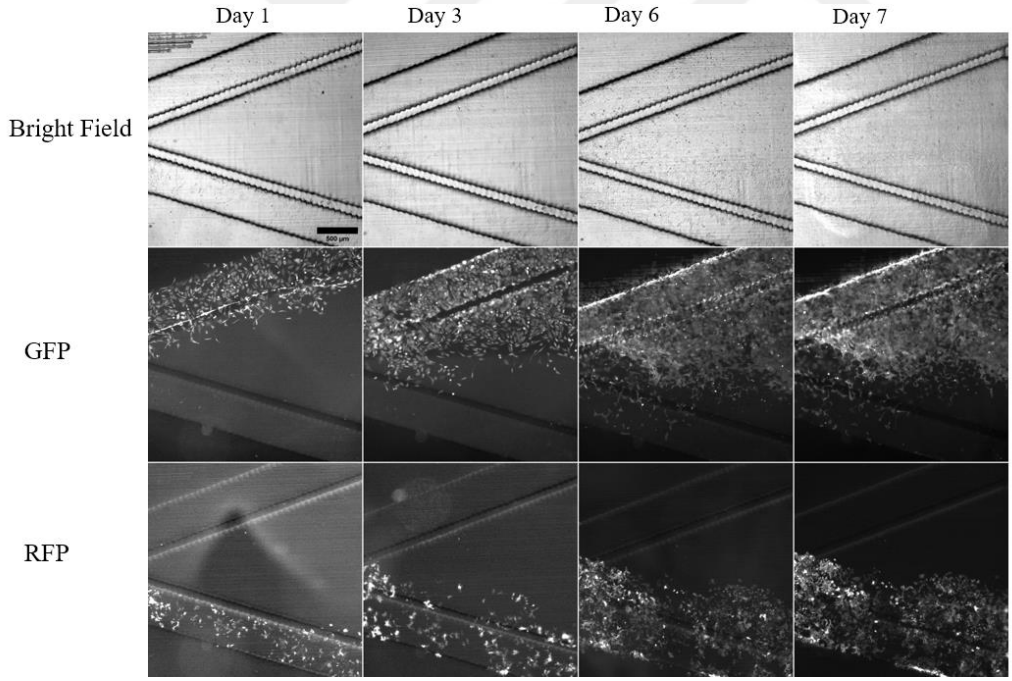

Figure 3.26 Fluorescent microscopy images of chip loaded with MCF-7 (bottom channel) and HMFU19 (top channel). Images are taken at 4X magnification and scale bar is 500 µm.

The same segmentation process applied to previous chips was also applied to variable width assays. However, to analyze the image in this variable width device, the image was divided into 5 different sections with same length to represent the gradually increasing distance between opposing channels. Sections are named with x coordinates (e.g. “section 500” corresponds to the section of the image that is 500 pixels away from image border). Below are the results.

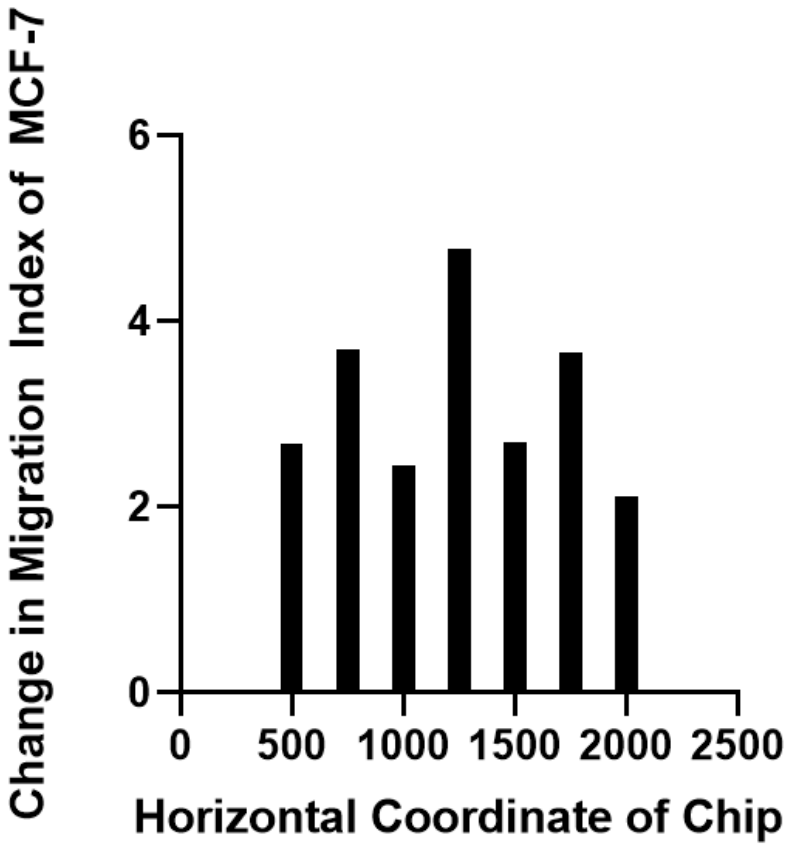

Figure 3.27 Plot showing the change in migration index of MCF-7 according to the distance to opposing channel which contains HMFU19 cells. 500 marks the section of the chip where two channels are closest, 2000 marks the section of the chip where two channels are farthest. The difference is taken between first and seventh days after seeding.

Afterwards, the same assay was repeated with MCF-7 cells but no other type of cells present in the culture.

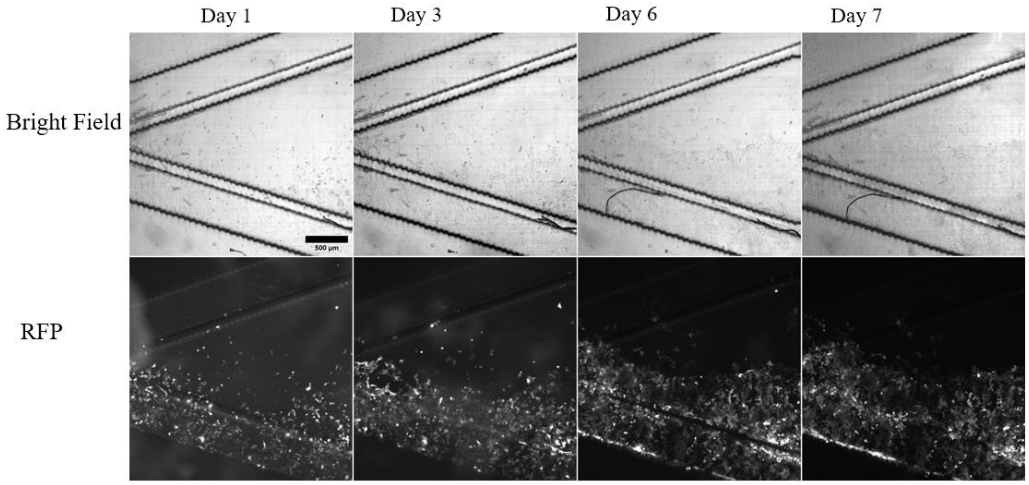

Figure 3.28 Fluorescent microscopy images of chip loaded with MCF-7 (bottom channel) and blank media (top channel). Images are taken at 4X magnification and scale bar is 500 µm.

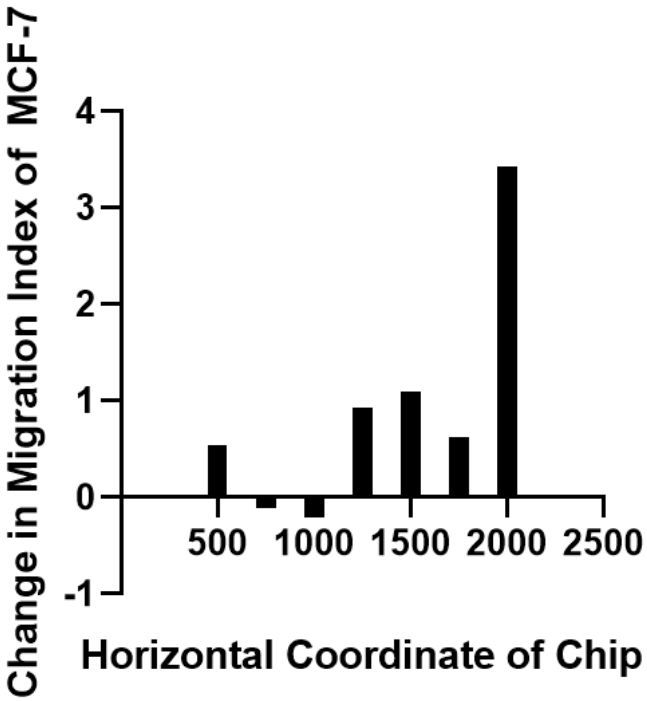

Figure 3.29 Plot showing the change in migration index of MCF-7 according to the distance to opposing channel which does not contain any cells. 500 marks the section of the chip where two channels are closest, 2000 marks the section of the chip where two channels are farthest. The difference is taken between first and seventh days after seeding.

From the segmentation data, it can be inferred that MCF-7 cells when cultured alone, do not display a very prominent migratory behaviour.

3.6 Variable Width Microchip Migration Assay Results for MDA-MB-231 Cells

As with co-culture chip, the same assays were repeated for MDA-MB-231 and HMFU19 cells.

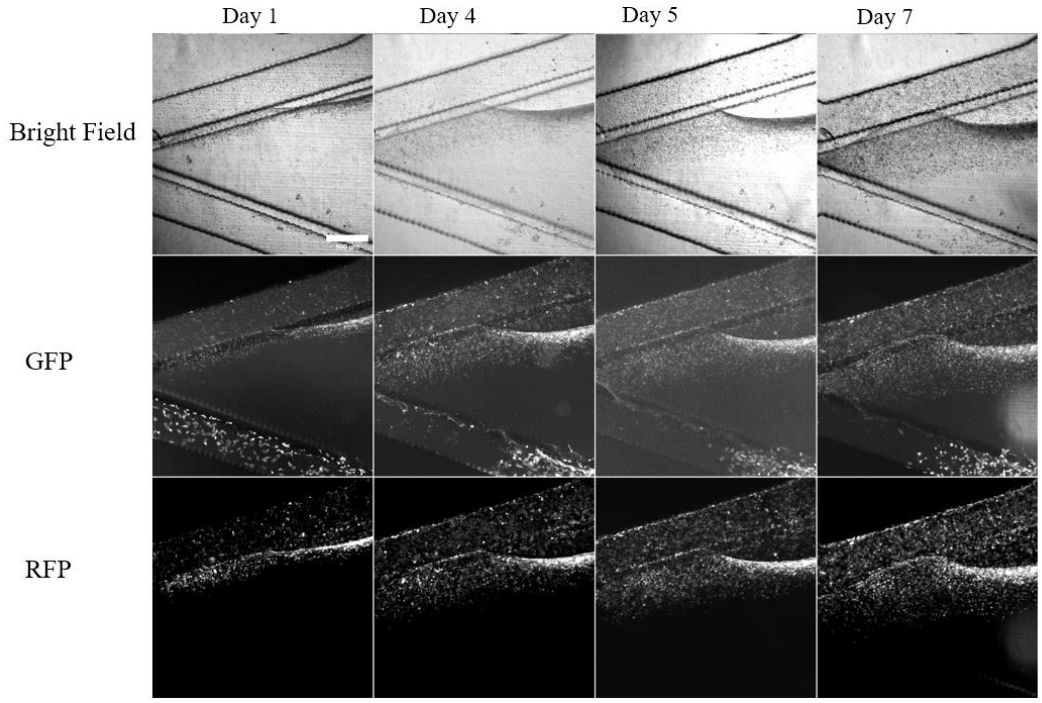

Figure 3.30 Fluorescent microscopy images of chip loaded with MDA-MB-231 upper channel) and HMFU19 (top channel). Images are taken at 4X magnification and scale bar is 500 μm.

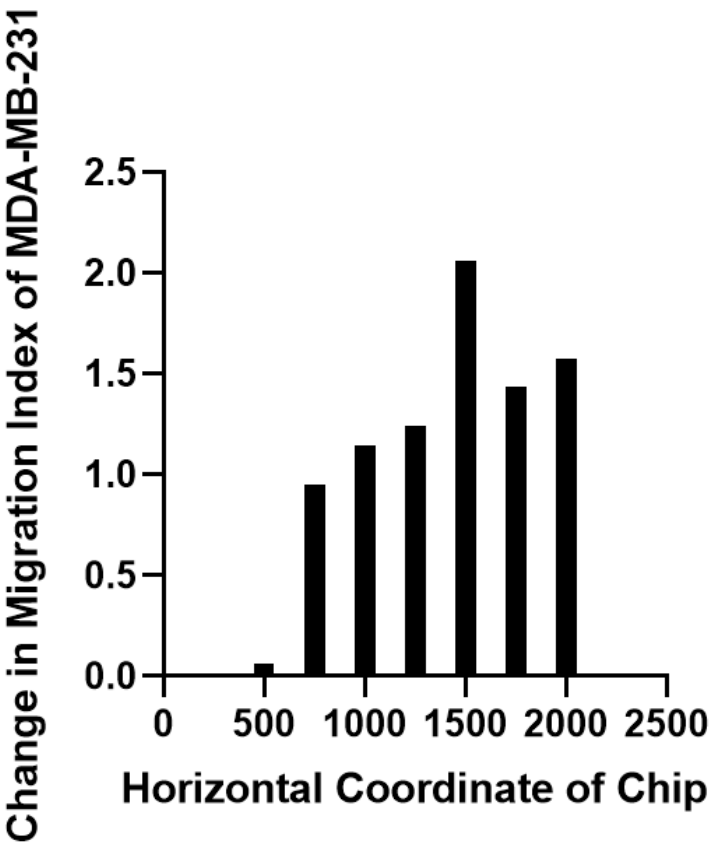

Figure 3.31 Plot showing the change in migration index of MDA-MB-231 according to the distance to opposing channel which contains HMFU19 any cells. 500 marks the section of the chip where two channels are closest, 2000 marks the section of the chip where two channels are farthest. The difference is taken between first and seventh days after seeding.

The same behaviour of MDA-MB-231 cells, that was pushing the collagen away from the walls, was also observed in this chip too. However, during the time between chip assays, MDA-MB-231 cells did develop an autofluorescence and that's the reason for the faint emission that is observed in GFP channel from MDA-MB-231 cells.

Though less prominent, a similar migration pattern to MCF-7 cells was also observed for MDA-MB-231 cells. The same experiments were repeated without the presence of any other type of cells.

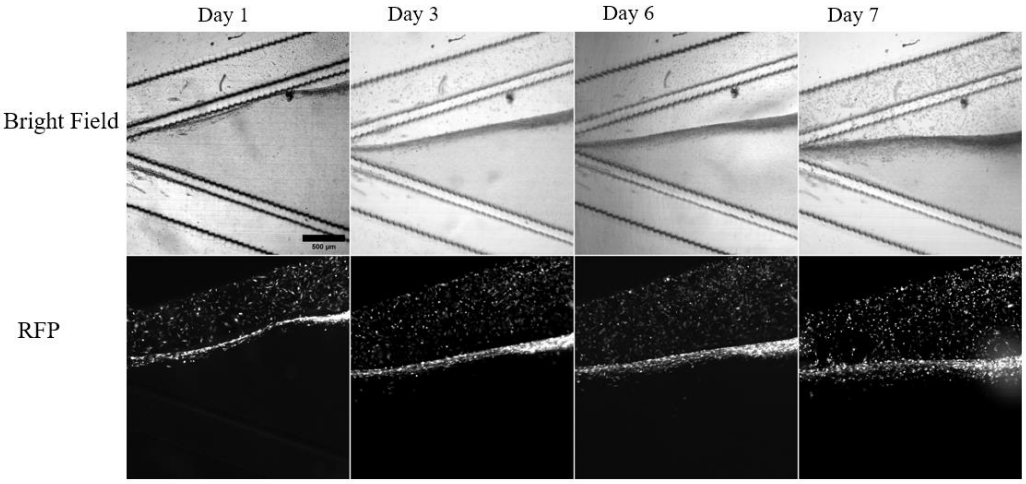

Figure 3.32 Fluorescent microscopy images of chip loaded with MDA-MB-231 cells (top channel) and blank media (bottom channel). Images are taken at 4X magnification and scale bar is 500 µm.

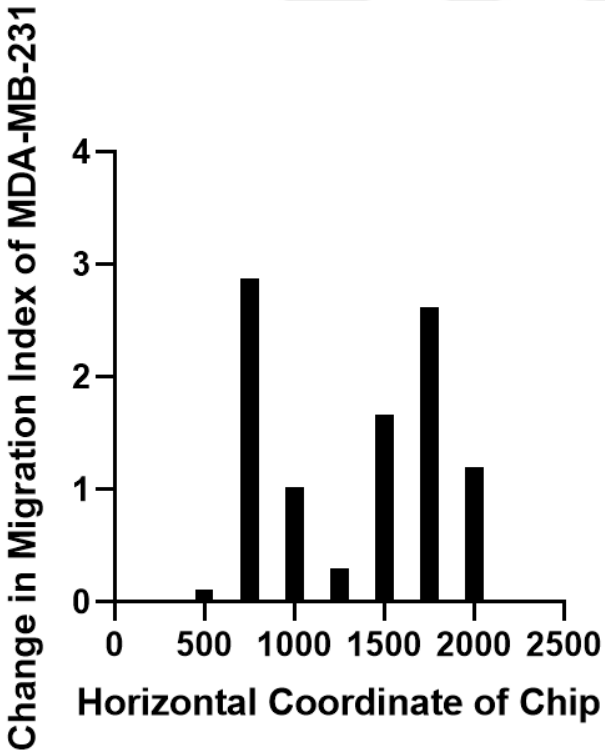

Figure 3.33 Plot showing the change in migration index of MDA-MB-231 according to the distance to opposing channel which does not contain any cells. 500 marks the section of the chip where two channels are closest, 2000 marks the section of the

chip where two channels are farthest. The difference is taken between first and seventh days after seeding.

The same collagen separation mentioned about MDA-MB-231 cells was also observed when they were cultured alone in the variable width microchip.

3.7 Variable Width Microchip Migration Assay Results for HMFU19 Cells

Microscopy images of HMFU19 cells when cultured with MDA-MB-231 and MCF-7 cells are displayed on Figure 3.37 and Figure 3.35 respectively. Below are the segmentation results of chips, analysed for HMFU19 cells.

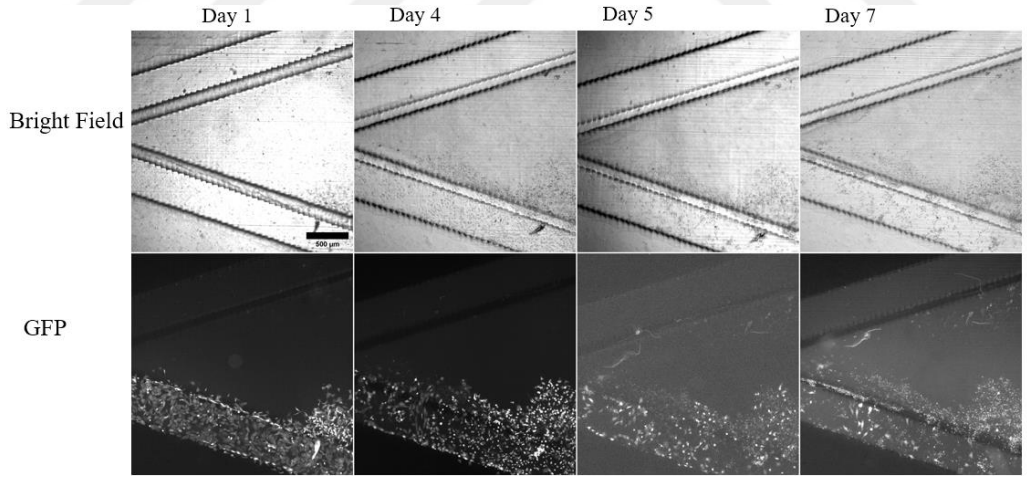

Figure 3.34 Fluorescent microscopy images of chip loaded with HMFU19 cells (bottom channel) and blank media (top channel). Images are taken at 4X magnification and scale bar is 500 µm.

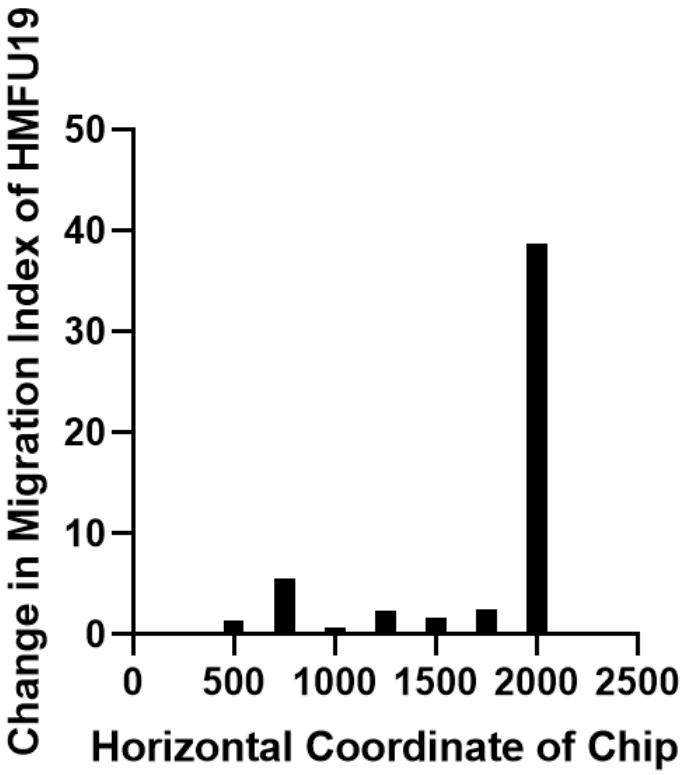

Figure 3.35 Plot showing the change in migration index of HMFU19 according to the distance to opposing channel which does not contain any cells. 500 marks the section of the chip where two channels are closest, 2000 marks the section of the chip where two channels are farthest. The difference is taken between first and seventh days after seeding.

CHAPTER 4

CONCLUSION

4.1 Findings and Discussion

As demonstrated by the finding of this study, a 3D printed microfluidic mold can be successfully used to culture different types of cells for enlengthened periods of time, showing the power of stereolithography. This conclusion can be drawn the fact from cells did not prematurely die or leak out of chips throughout the culture which can be seen in the microscopy images.

Also, the analysis results show that MDA-MB-231 and MCF-7 cells do not show a very considerable change in their migratory behaviour when cultured with HMFU19 cells, compared to their mono culture conditions. However, even the linear regression analysis shows that their rate of migration is affected by the presence of HMFU19 cells by increasing.

The migratory behaviour of HMFU19 cells on the other hand seems to be getting affected more by the presence of a breast cancer cell (MDA-MB-231 or MCF-7 in this study).

Liu and Mak (2022) found that when cultured with found that fibroblasts make MDA-MB-231 cells more motile, possibly by altering ECM components. However, they have also observed when cultured with fibroblasts cancer cells gain a more elongated physiology when compared to mono-culture conditions. From this point, since no such phenomenon observed in our experiments (however it must be noted that we did not do such an analysis for this behaviour), combined with the results of cancer cells not showing a drastic change in migration, it might be suggested that

maybe cancer cells do not recognize the presence or get affected by fibroblasts possibly due to the rather long distance between cells.

Miyazaki et al. (2019) showed that fibroblasts enhance the migration of cancer cells by providing attachment points to them. However, in contrast to our study again, the fibroblasts and cancer cells are in very close proximity to fibroblasts. Therefore, the reason for us not seeing a drastic change in migration of cancer cells might be due to the distance between seeding channels.

In contrast, to our findings Morgan, H., & Hill, P. A. (2005) found similar levels of collagen I matrix degradation between MCF-7 and MDA-MB-231 cell line when cultured with serum containing media. Therefore, the collagen separation seen exclusively in MDA-MB-231 experiments in our research can be attributed to MDA-MB-231 cells physically pushing the collagen rather than biochemically degrading it.

Experiments done with variable width device show that the migration pattern of cells actually change slightly according to the distance to the opposing channel. However, there is not a clear pattern demonstrated. To clarify the situation, more experiments with the same device should be done. Results shown in this project are not adequate to set up a clear claim.

4.2 Limitations of the Study

Since the chips used in this project were all 3D printed, there are some shortcomings resulting from this process. For example, generally surface roughness of such chips are higher compared to photo lithography produced chips, resulting in containment issues, lowering the amount of successful chips produced. Moreover, some pixel resolution issues were observed after producing the molds. As mentioned before there are some differences between designed parameters and manufactured molds. There were some problems with chips bonding to glass slides present, probably again

resulting from the rather higher surface roughness of 3D printed molds. Also, in order to take the micrographs of chips, they needed to be taken out of sterile working conditions and placed under the microscope, making them quite vulnerable to contamination. These are the areas that can be improved fort his study.

Since it was observed that MDA-MB-231 cells disrupt the collagen gel during their migration, their quantitative result might not be directly compared to MCF-7 cells. In order to rectify this situation, different types of gels such as alginate might be used to fill the middle layer.

4.3 Future Prospects

In order to reveal the differences between CAFs and normal fibroblasts in terms of how they affect cancer cells, same assays can be repeated using CAFs instead of HMFU19 cells and results can be compared. In this project, we have also investigated the effects of CAFs on MCF-7 and MDA-MB-231 cells in terms of growth, instead of migration.

To achieve this, 544-CAF (a breast cancer associated fibroblast cell line) cells were embedded in a collagen matrix and seeded into the middle channel of the co-culture chip mentioned previously. On cellular channels (top and bottom channels), CAFs and HMFU cells were seeded, and their growth was compared to the condition where no other type of cell was present. To perform this, the fluorescent signal emitting area in the middle channel was counted using Fiji software. Below are the preliminary result of this experiment.

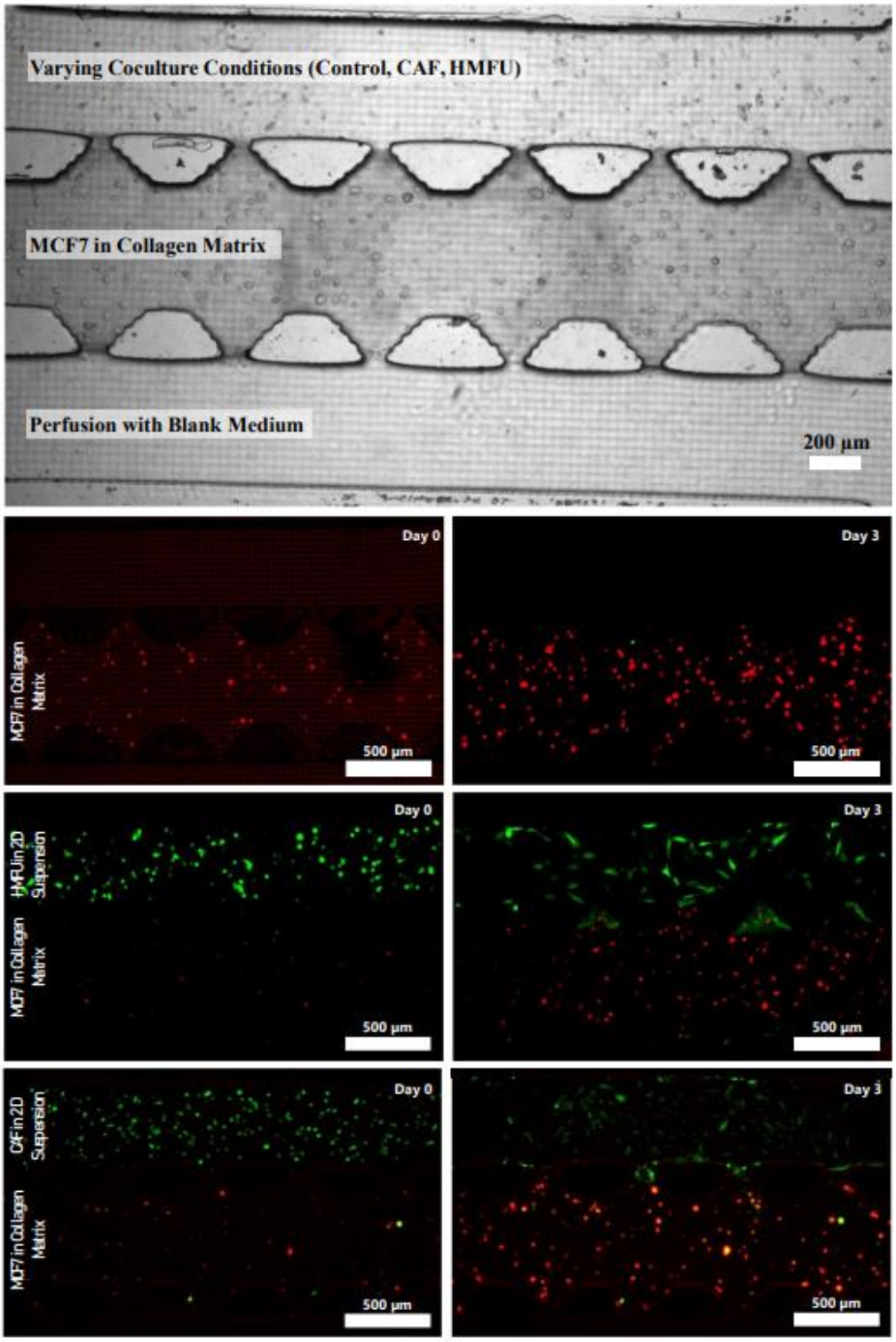

Figure 4.1 Showing the growth of MCF-7 cells in 3D collagen (middle layer) in different configurations, showing the change in growth rate when cultured alone,

with 544CAFs and with HFMU19 cells. (taken from Barış Dedekargınoğlu's master thesis)

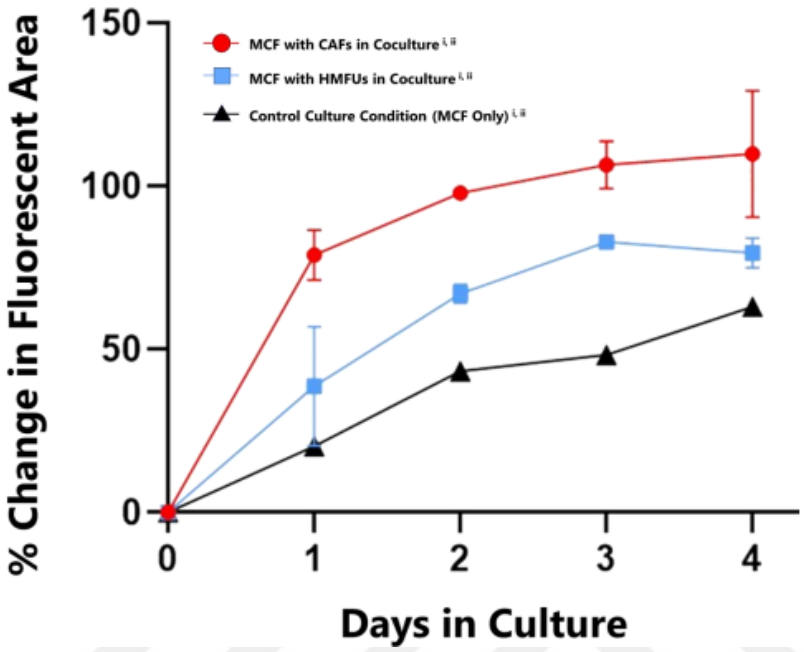

Figure 4.2 Plot showing the difference in growth rate of MCF-7 when cultured in different configurations, showing that MCF-7 cells grow the fastest when cultured with 544CAF cells (taken from Barış Dedekargınoğlu's master's thesis).

REFERENCES

Atkins, T., & Escudier, M. (2013). A Dictionary of Mechanical Engineering. In *Oxford University Press eBooks*. https://doi.org/10.1093/acref/9780199587438.001.0001.

Convery, N., & Gadegaard, N. (2019). 30 years of microfluidics. *Micro and Nano Engineering*, *2*, 76–91. https://doi.org/10.1016/j.mne.2019.01.003.

Gharib, G., Bütün, İ., Muganlı, Z., Kozalak, G., Namlı, İ., Sarraf, S. S., Ahmadi, V. E., Toyran, E., Van Wijnen, A. J., & Koşar, A. (2022). Biomedical Applications of Microfluidic Devices: A review. *Biosensors*, *12*(11), 1023. https://doi.org/10.3390/bios12111023.

Zhang, Z., & Nagrath, S. (2013). Microfluidics and cancer: are we there yet?. *Biomedical microdevices*, *15*(4), 595–609. https://doi.org/10.1007/s10544-012-9734-8.

Scott, S. M., & Ali, Z. (2021). Fabrication Methods for Microfluidic Devices: An Overview. *Micromachines*, *12*(3), 319. https://doi.org/10.3390/mi12030319.

Comșa, Ș., Cîmpean, A. M., & Raica, M. (2015). The Story of MCF-7 Breast Cancer Cell Line: 40 years of Experience in Research. *Anticancer research*, *35*(6), 3147–3154.

Welsh, J. (2013). Animal models for studying prevention and treatment of breast cancer. In Elsevier eBooks (pp. 997–1018). https://doi.org/10.1016/b978-0-12-415894-8.00040-3.

O'Hare, M. J., Bond, J., Clarke, C., Takeuchi, Y., Atherton, A. J., Berry, C., Moody, J., Silver, A. R., Davies, D. C., Alsop, A. E., Neville, A. M., & Jat, P. S. (2001). Conditional immortalization of freshly isolated human mammary fibroblasts and endothelial cells. Proceedings of the National Academy of Sciences of the United States of America, 98(2), 646–651. https://doi.org/10.1073/pnas.98.2.646.

Lin, L., & Chung, C. K. (2021). PDMS Microfabrication and Design for Microfluidics and Sustainable Energy Application: Review. *Micromachines*, *12*(11), 1350. https://doi.org/10.3390/mi12111350.

Regmi, S., Poudel, C., Adhikari, R., & Luo, K. Q. (2022). Applications of Microfluidics and Organ-on-a-Chip in Cancer Research. *Biosensors*, *12*(7), 459. https://doi.org/10.3390/bios12070459

Wu, J. S., Jiang, J., Chen, B. J., Wang, K., Tang, Y. L., & Liang, X. H. (2021). Plasticity of cancer cell invasion: Patterns and mechanisms. *Translational oncology*, *14*(1), 100899. https://doi.org/10.1016/j.tranon.2020.100899.

Plikus, M. V., Wang, X., Sinha, S., Forte, E., Thompson, S. M., Herzog, E. L., Driskell, R. R., Rosenthal, N., Biernaskie, J., & Horsley, V. (2021). Fibroblasts: Origins, definitions, and functions in health and disease. *Cell*, *184*(15), 3852–3872. https://doi.org/10.1016/j.cell.2021.06.024.

Yang, D., Liu, J., Qian, H. *et al.* Cancer-associated fibroblasts: from basic science to anticancer therapy. *Exp Mol Med* **55**, 1322–1332 (2023). https://doi.org/10.1038/s12276-023-01013-0.

Ping, Q., Yan, R., Cheng, X. *et al.* Cancer-associated fibroblasts: overview, progress, challenges, and directions. *Cancer Gene Ther* **28**, 984–999 (2021). https://doi.org/10.1038/s41417-021-00318-4.

Borók, A., Laboda, K., & Bonyár, A. (2021). PDMS Bonding Technologies for Microfluidic Applications: A Review. *Biosensors*, *11*(8), 292. https://doi.org/10.3390/bios11080292.

Miranda, I., Souza, A., Sousa, P., Ribeiro, J., Castanheira, E. M. S., Lima, R., & Minas, G. (2021). Properties and Applications of PDMS for Biomedical

Engineering: A Review. *Journal of functional biomaterials*, *13*(1), 2. https://doi.org/10.3390/jfb13010002.

Ariati, R., Sales, F., Souza, A., Lima, R. A., & Ribeiro, J. (2021). Polydimethylsiloxane Composites Characterization and Its Applications: A Review. Polymers, 13(23), 4258. https://doi.org/10.3390/polym13234258.

Zhai, J., Liu, Y., Ji, W., Huang, X., Wang, P., Li, Y., Li, H., Wong, A. H., Zhou, X., Chen, P., Wang, L., Yang, N., Chen, C., Chen, H., Mak, P., Deng, C., Martins, R., Yang, M., Ho, T., . . . Jia, Y. (2024). Drug screening on digital microfluidics for cancer precision medicine. Nature Communications, 15(1). https://doi.org/10.1038/s41467-024-48616-3.

Novikov, N. M., Zolotaryova, S. Y., Gautreau, A. M., & Denisov, E. V. (2020). Mutational drivers of cancer cell migration and invasion. British Journal of Cancer, 124(1), 102–114. https://doi.org/10.1038/s41416-020-01149-0.

Friedl, P., & Gilmour, D. (2009). Collective cell migration in morphogenesis, regeneration and cancer. Nature Reviews Molecular Cell Biology, 10(7), 445–457. https://doi.org/10.1038/nrm2720.

Fares, J., Fares, M. Y., Khachfe, H. H., Salhab, H. A., & Fares, Y. (2020). Molecular principles of metastasis: a hallmark of cancer revisited. Signal

Transduction and Targeted Therapy, 5(1). https://doi.org/10.1038/s41392-020-0134-x.

Nielsen, A. V., Beauchamp, M. J., Nordin, G. P., & Woolley, A. T. (2020). 3D printed microfluidics. Annual Review of Analytical Chemistry, 13(1), 45–65. https://doi.org/10.1146/annurev-anchem-091619-102649.

Bhattacharjee, N., Urrios, A., Kang, S., & Folch, A. (2016). The upcoming 3D-printing revolution in microfluidics. Lab on a Chip, 16(10), 1720–1742. https://doi.org/10.1039/c6lc00163g.

Jeong, S., Lee, J., Shin, Y., Chung, S., & Kuh, H. (2016). Co-Culture of tumor spheroids and fibroblasts in a collagen Matrix-Incorporated microfluidic chip mimics reciprocal activation in solid tumor microenvironment. PLoS ONE, 11(7), e0159013. https://doi.org/10.1371/journal.pone.0159013.

Firatligil-Yildirir, B., Bati-Ayaz, G., Tahmaz, I., Bilgen, M., Pesen-Okvur, D., & Yalcin-Ozuysal, O. (2021). On-chip determination of tissue-specific metastatic potential of breast cancer cells. Biotechnology and Bioengineering, 118(10), 3799–3810. https://doi.org/10.1002/bit.27855.

Azadi, S., Shadpour, M. T., & Warkiani, M. E. (2020). Characterizing the effect of substrate stiffness on the extravasation potential of breast cancer cells using a 3D

microfluidic model. Biotechnology and Bioengineering, 118(2), 823–835. https://doi.org/10.1002/bit.27612.

Kalluri, R., & Zeisberg, M. (2006). Fibroblasts in cancer. Nature Reviews. Cancer, 6(5), 392–401. https://doi.org/10.1038/nrc1877.

Guo, X., Chen, M., Cao, L., Hu, Y., Li, X., Zhang, Q., Ren, Y., Wu, X., Meng, Z., & Xu, K. (2021). Cancer-Associated fibroblasts promote migration and invasion of Non-Small cell lung cancer cells via MIR-101-3P mediated VEGFA secretion and AKT/ENOS pathway. Frontiers in Cell and Developmental Biology, 9. https://doi.org/10.3389/fcell.2021.764151.

Kapałczyńska, M., Kolenda, T., Przybyła, W., Zajączkowska, M., Teresiak, A., Filas, V., Ibbs, M., Bliźniak, R., Łuczewski, Ł., & Lamperska, K. (2016). 2D and 3D cell cultures – a comparison of different types of cancer cell cultures. Archives of Medical Science. https://doi.org/10.5114/aoms.2016.63743.

Yamamoto, Y., Kasashima, H., Fukui, Y., Tsujio, G., Yashiro, M., & Maeda, K. (2022). The heterogeneity of cancer-associated fibroblast subpopulations: Their origins, biomarkers, and roles in the tumor microenvironment. Cancer Science, 114(1), 16–24. https://doi.org/10.1111/cas.15609.

Parsian, M., Mutlu, P., Yildirim, E., Ildiz, C., Ozen, C., & Gunduz, U. (2022). Development of a microfluidic platform to maintain viability of micro-dissected tumor slices in culture. Biomicrofluidics, 16(3). https://doi.org/10.1063/5.0087532.

Truong, D. D., Kratz, A., Park, J. G., Barrientos, E. S., Saini, H., Nguyen, T., Pockaj, B., Mouneimne, G., LaBaer, J., & Nikkhah, M. (2019). A Human Organotypic Microfluidic Tumor Model Permits Investigation of the Interplay between Patient-Derived Fibroblasts and Breast Cancer Cells. Cancer Research, 79(12), 3139–3151. https://doi.org/10.1158/0008-5472.can-18-2293.

Vasudevan, J., Lim, C. T., & Fernandez, J. G. (2020). Cell Migration and Breast Cancer Metastasis in Biomimetic Extracellular Matrices with Independently Tunable Stiffness. Advanced Functional Materials, 30(49). https://doi.org/10.1002/adfm.202005383.

Dedekargınoğlu, B. (2023). RAPID PROTOTYPING OF MICROFLUIDIC TISSUE CULTURE SYSTEMS VIA MASK BASED PHOTO POLYMERIZATION [Master's Thesis]. Middle East Technical University

Liu, C., & Mak, M. (2022). Fibroblast-mediated uncaging of cancer cells and dynamic evolution of the physical microenvironment. Scientific Reports, 12(1). https://doi.org/10.1038/s41598-021-03134-w.

Miyazaki, K., Oyanagi, J., Hoshino, D., Togo, S., Kumagai, H., & Miyagi, Y. (2019). Cancer cell migration on elongate protrusions of fibroblasts in collagen matrix. Scientific Reports, 9(1). https://doi.org/10.1038/s41598-018-36646-z.

Morgan, H., & Hill, P. A. (2005). Human breast cancer cell-mediated bone collagen degradation requires plasminogen activation and matrix metalloproteinase activity. Cancer cell international, 5(1), 1. https://doi.org/10.1186/1475-2867-5-1.